Vulnerability in a Tropical Cyclone Risk Model: Philippines Case Study

Jane W. Baldwin*

Department of Earth System Science, University of California Irvine, Irvine, California

Chia-Ying Lee

Lamont-Doherty Earth Observatory, Palisades, New York

Brian J. Walsh

World Bank, Washington, D.C.

Suzana J. Camargo

Lamont-Doherty Earth Observatory, Palisades, New York

Adam H. Sobel

Columbia University, New York, New York

Corresponding author: Jane W. Baldwin, jane.baldwin@uci.edu

ABSTRACT

The authors describe a tropical cyclone risk model for the Philippines, using methods that are open-source and can be straightforwardly generalized to other countries. Wind fields derived from historical observations, as well as those from an environmentally forced tropical cyclone hazard model (using environmental forcing from the recent historical period) are combined with data representing exposed value and vulnerability to determine asset losses. Exposed value is represented by the LitPop dataset, which assumes total asset value is distributed across a country following population density and nightlights data. Vulnerability is assumed to follow a functional form previously proposed by Emanuel, with free parameters chosen by a sensitivity analysis in which simulated and historical reported damages are compared for different parameter values. Use of different vulnerability parameters for the region around Manila yields much better agreement between simulated and actually reported losses than does a single set of parameters for the entire country. Even then, however, the model predicts no losses for a substantial number of historical storms which did in fact produce them, a difference the authors hypothesize is at least in part due to the use of wind speed as the sole metric of TC hazard, omitting explicit representation of flooding due to storm surge and/or rainfall.

Significance statement. Landfalling tropical cyclones are devastating disasters in terms of their loss of property and life. The Philippines is particularly at risk for these disasters. Here we develop a model for tropical cyclone risk, e.g. property losses, over the Philippines, and demonstrate its effectiveness by comparing to historical observations. We find that capturing the difference in vulnerability between the largest city in the Philippines (Manila) and more rural areas is important to accurately model tropical cyclone risks. Using this model, we can more accurately simulate the risk of very extreme tropical cyclone events in the Philippines. The model can also easily be applied to other countries and for climate change scenarios using information that is openly available. Our model does not accurately capture damages from storms dominated by flooding instead of wind, and future work should improve this aspect of the model. Nonetheless, the existing model is useful for emergency planning and adaptation, especially in lower income countries where data is limited.

1. Introduction

Accurate assessments of tropical cyclone (TC) risk are valuable for disaster risk reduction and climate adaptation. Such assessments can inform decisions about both where to build resilience and emergency preparedness prior to TC-induced disasters and where to allocate aid following such disasters, and can also inform the development of insurance and reinsurance products. Assessing risk requires consideration of three different factors (Field et al. 2012). The first factor is the hazard. The hazard characterizes the probabilities that given levels of geophysical variables — e.g., wind speed, rainfall, storm surge — will be exceeded. The second factor is the exposure, which characterizes the human, structural, or agricultural assets in a place which might be affected by the disaster. The third factor is vulnerability, which is the degree to which those assets will be lost if one or more of the geophysical variables exceeds a given value. TC risks are typically quantified in the form of asset losses, or the replacement cost of assets destroyed by a TC event.

Over the past decade or so, significant strides have been made in quantifying different aspects of TC risk. Given that TCs — particularly the few most intense ones that cause the largest share of damage — are rare events, the observed historical record is too limited for accurate TC risk assessment. Statistical-dynamical models have been developed that allow the simulation of many physically plausible TCs given background environmental conditions (Emanuel 2011; Lee et al. 2018; Jing and Lin 2020; Bloemendaal et al. 2020b). Synthetic TCs generated by such models are used for assessment of extreme wind hazards (Sobel et al. 2019; Bloemendaal et al. 2020a), coupled with hydrodynamical models to estimate storm surge hazards (Lin et al. 2010; Lin and Chavas 2012), and coupled with physics-based models of precipitation to estimate extreme rainfall hazards (Xi et al. 2020; Gori et al. 2022).

Alongside these advances in modeling TC hazards, progress has been made in modeling TC vulnerability and exposure. This work can be broadly categorized into structural, economic, and social approaches (Wilson and Baldwin 2021). For the USA, FEMA's Hazus model provides a relatively comprehensive framework for modeling wind and flood risks, including computation of exposure and vulnerability from building maps and structural engineering principles (Vickery et al. 2006b,a). Some information in Hazus, especially around vulnerability of building types, has been adapted for use in other countries by the UNISDR's Global Assessment Reports (Yamin et al. 2014). However, the lack of detailed building maps and complexity of Hazus does limit its applicability to other countries. In contrast, recent studies using more top-down, economic-based approaches have created global exposure fields and country-scale impact functions for TC risk modeling (Eberenz et al. 2020b,a). While these methods are more simplified than Hazus, they have the advantage of being consistently applicable across the globe. Vulnerability can also be estimated based on population characteristics (what we term "social approaches") (Cutter et al. 2003; Tellman et al. 2020; Dominguez et al. 2021). While these techniques are suitable for assessing relative

vulnerabilities of different regions (e.g. counties), existing social approaches are somewhat less straightforward to merge with TC hazard and exposure for quantitative risk assessment.

A key challenge for TC risk assessment is incorporating changing hazards following climate change. As carbon concentrations in the atmosphere increase and the global climate warms, TCs and their related hazards may be altered in a variety of ways. There is high confidence that rising sea levels will lead to greater storm surge, medium to high confidence that TC-related precipitation will increase, and medium to high confidence that TC intensity will increase (Knutson et al. 2020). Other aspects of TC change are more uncertain. For example, there is ongoing debate about how the overall frequency of TCs will change with global warming (Vecchi et al. 2019), though somewhat more confidence that the frequency of the most intense (i.e. Category 4 or 5 storms) will increase. Traditionally, hurricane risk assessment has been based primarily on historical tracks (Watson and Johnson 2004), but this approach is not appropriate in a non-stationary climate. In contrast, the previously discussed statistical-dynamical approaches can be applied with environmental conditions drawn from climate change scenarios to estimate changing hazards from TCs (Emanuel 2011; Lee et al. 2020); this method presents an important way forwards in estimating present and future TC risk. However, to fully capture TC risks in a changing climate also requires consideration of the compound hazards associated with these storms (Leonard et al. 2014; Zscheischler et al. 2018). Wind, precipitation, surge, rising temperatures and sea levels all play roles in changing TC risks and studies are beginning to consider these changing hazards in concert (Lin et al. 2012; Matthews et al. 2019; Gori et al. 2022).

Another challenge for TC risk assessment, and disaster risk assessment in general, is quantitatively capturing impacts on human welfare. Disasters have been shown to disproportionately effect poorer countries (Noy 2009). In the Philippines in particular, typhoons disproportionately effect poorer individuals and children, in terms of educational, economic, and health impacts (Deuchert

and Felfe 2015; Sakai et al. 2017; Yonson et al. 2018). Traditional quantification of asset losses cannot account for these differential impacts across the income distribution. Indeed, asset losses may more readily reflect the impact on wealthy individuals who own the most assets, as opposed to poorer individuals whose welfare can be more gravely affected by a given disaster (Hallegatte et al. 2016). Fortunately, recent studies have provided novel frameworks to rigorously quantify welfare impacts of disasters. For example, Walsh and Hallegatte (2019) employed agent-based modeling of consumption changes at the household level to quantify impacts of historical disasters in the Philippines; this study finds that Filipinos in the bottom income quintile experience 9% of the asset losses from these events but 31% of the wellbeing losses. Further work is needed to estimate wellbeing impacts of disasters in a changing climate.

In this study, we focus on TC risk assessment for the Philippines largely because this country experiences particularly high risks from these events. About 70% of Western North Pacific typhoons form in or enter the region directly surrounding the Philippines (Corporal-Lodangco and Leslie 2017). The more active period for TCs is June through December, during which time the median number of Philippines landfalls is six (Corporal-Lodangco and Leslie 2017). Around the Philippines, ENSO plays a dominant role in year-to-year variability of TC genesis frequency, tracks, and associated precipitation (Lyon and Camargo 2009; Corporal-Lodangco et al. 2016), and has been implicated in the formation of exceedingly strong storms (Lin et al. 2014).

Landfalling typhoons in the Philippines are disasters both in terms of economic impacts and fatalities (Ribera et al. 2008; Walsh and Hallegatte 2019). Recent storms have highlighted these dangers. In 2013, Typhoon Haiyan made landfall in the Philippines as a Category 5 storm, but with maximum sustained winds exceeding the threshold for Category 5 by over 18 m/s (Lin et al. 2014). The extremely strong winds were accompanied by very high velocity surges and resultant flooding (Soria et al. 2016). The storm made a direct hit to Eastern Visayas, a region on the eastern

side of the Philippines. Haiyan is estimated to have cost the Philippines 13 billion USD (Ehrhart et al. 2014), and resulted in 6,300 known fatalities, the vast majority occurring in Eastern Visayas, with an additional 1,062 individuals missing and 28,688 injured (del Rosario). These impacts were exacerbated by large populations living along the coast in structurally vulnerable (wood or bamboo) housing (Mas et al. 2015; Eadie et al. 2020). For perspective, Hurricane Katrina resulted in 1,833 known fatalities and several hundred persons missing in the USA (Beven et al. 2008). Very recently, in December 2021, Typhoon Rai (Odette) made multiple landfalls in the Southern Philippines with an initial intensity of Category 5, causing widespread flooding. This disaster is the third costliest typhoon in Philippines history, affecting an estimated 12 million people and causing greater then 400 fatalities (OCHA 2022).

There is a strong need for accurate TC risk assessment in the Philippines to support disaster risk reduction and management efforts. However, assessment of TC risk in the Philippines is complicated by opposing spatial gradients of hazard and socioeconomic vulnerability (Figure 1). The northern Philippines experiences more frequent TCs than does the southern Philippines, but is also wealthier and more socioeconomically resilient, meaning better able to cope with and recover from disaster asset losses. The city of Manila and its surroundings (also called the National Capital Region or NCR), constitute by far the most populated and developed region in the Philippines. In contrast, the southern Philippines is generally poorer and less socioeconomically resilient. Socioeconomic resilience is defined here as the ratio of expected asset losses to wellbeing losses as in Walsh and Hallegatte (2020). These opposing patterns of hazard and resilience pose a dilemma for the Philippines itself and international agencies (such as the World Bank) aiming to distribute aid for disaster risk reduction. Should this aid focus on the northern Philippines, where exposure and hazards, and in turn asset losses, are greatest, or on the southern Philippines, which is more vulnerable and where the human wellbeing losses may be greatest? To answer this question requires

rigorous TC risk assessment that accurately models differences in losses across the Philippines, and, ultimately, consideration of losses across the income distribution.

The primary goal of the present work is to produce and validate an open-source TC risk model for the Philippines. To do so requires the development of layers for hazard, exposure, and vulnerability using methods based on publicly available data. Here we detail the development of this model. We focus on sensitivity of the results to vulnerability, as vulnerability is the component of the model that is least constrained by observational data. In particular, we demonstrate that using vulnerability that varies by region substantially improves the accuracy of TC risk estimates compared to prior country-scale analyses. We develop layers for vulnerability and exposure to combine with TC tracks from the Columbia tropical cyclone Hazard model (CHAZ), as well as with those from historical observations. CHAZ is a statistical-dynamical tropical cyclone model that can generate many physically plausible synthetic TCs based on background environmental conditions, allowing evaluation of TC risks out to longer return periods than are available from the historical record alone (Lee et al. 2018). The performance of CHAZ is comparable to that of other stochastic TC hazard models, including in the West Pacific (Meiler et al. 2022). For exposure, we employ an existing global dataset of asset value called LitPop that depends on population and nightlights data (Eberenz et al. 2020b). Finally, for vulnerability we fit parameters for an existing vulnerability function (Emanuel 2011) at the regional level by combining information on damages and wind swaths for historical TCs with data on household construction materials. In the Philippines “region" is the name for a particular administrative division; the country is divided into 17 regions (shown in center panel of Figure 1), which are further subdivided into 81 provinces. For some results, we focus on two regions as contrasting examples: 1) the National Capital Region (NCR), which contains Manila and is highly urbanized, and 2) Eastern Visayas, a relatively less affluent region that was directly impacted by Haiyan.

While we focus on the Philippines, the second goal of the paper is to develop a methodology that can be employed more broadly. CHAZ is global, as is LitPop, and the approach we take to vulnerability can also be applied elsewhere. While the model we develop here can be used as a stand-alone model for the Philippines, we also view it as a pilot study for the development of a global, open-source tropical cyclone risk model based on CHAZ.

The rest of this paper is structured as follows. Section 2 describes the methods and datasets used in this work. Section 3 shows the sensitivity of risk estimates to different assumptions about vulnerability. Section 4 applies this risk model to create TC risk estimates for the Philippines based on CHAZ. Finally, Section 5 ends this paper with a summary and conclusions.

2. Methods

Our workflow combines hazard, vulnerability, and exposure to calculate asset losses from TCs in the Philippines (Figure 2), and validates those asset losses against observations from historical storms. We describe the basic methods we use to determine each risk component separately here, and discuss vulnerability further in the next section.

a. Hazard

We make the simplifying assumption that total TC losses can be modeled as a function of wind speed. In reality, TCs cause losses through a number of different additional sub-perils associated with these events including intense rainfall, storm surge, and their associated flooding and landslides (Cinco et al. 2016). Rainfall and storm surge are only indirectly and loosely related to wind speed; for example, some relatively weak but slow moving storms can result in large amounts of rainfall (Sato and Nakasu 2011). However, due to additional complexities involved

in modeling rainfall and storm surge, wind speed is often used as a first order estimate of TC hazard (Eberenz et al. 2020a; Emanuel 2011).

We use two different types of TC track data. The first comprises historical TC tracks from the International Best Track Archive for Climate Stewardship (IBTrACS, v04r00). This version includes data from a number of different meteorological agencies across the world (Knapp et al. 2010). Given that multiple agencies may provide track and intensity data for a particular storm, we choose to examine Western North Pacific track data from only the Joint Typhoon Warning Center (JTWC). Philippines-landfalling storms recorded in this dataset span the year 1945 to the present. The second data source consists of synthetic tracks from CHAZ, specifically those produced using environmental fields from the ERA-Interim reanalysis (Dee et al. 2011; Lee et al. 2018). Both the historical and CHAZ tracks are available at 6-hourly temporal resolution. We extract the salient information from these tracks (latitude, longitude, maximum sustained wind speed) and linearly interpolate them to a 15-min temporal resolution. We use tracks that make a landfall in the Philippines, determined by the intersection of these 15-min resolution track points with a 5 arc-minute resolution land mask of this country. In IBTrACS, there are 480 historical Philippines-landfalling tropical cyclones. Downscaled from ERA-Interim, CHAZ generated in total 94,500 synthetic storms making landfall in the Philippines. This number includes 3178 storm tracks and each track has roughly 30 stochastically generated intensification trajectories (Lee et al. 2016, 2018). For each of these landfalling storms, we use data extending from one day before the first landfall to one day after the last landfall in the Philippines for our risk analysis. Samples of landfalling TC tracks from IBTrACS and CHAZ are shown in Figure 3. Across the two sets of TCs, locations of landfall and distribution of intensities at first landfall are similar. However, CHAZ synthetic TCs do not last as long after passing through the Philippines as IBTrACS observed TCs, and are directed more southward.

A TC track consists of a set of points defining a one-dimensional curve in time and space, with the wind represented by a single number, the maximum sustained wind speed. It is necessary to generate two-dimensional wind swaths at each point along the track, in order to use those winds, together with spatially varying exposure and vulnerability data, to model damage. Swaths should account for the variation of wind speed from the center of the storm, and some asymmetries typical in TCs. To do this, we employ an approach based on previously published parametric wind models, described below and summarized in Figure 4. An important input to this modeling approach is the radius of maximum wind (RMW). In IBTrACS, observed estimates of RMW are available for some but not all storms. As a result, we estimate RMW using the empirically-derived Knaff et al. (2015) formula, in which the predicted RMW depends on latitude and maximum sustained wind speed. This formula was developed using data from the North Atlantic basin, where storms typically do not reach intensities as high as those in the Western North Pacific basin. A side effect of this difference is that the formula produces physically unreasonable RMW values (extremely small or negative) for the strongest storms observed around the Philippines. To compensate for this issue, any RMW values predicted by the formula to be less than 20 km are overridden to be 20 km, which is on the lower end of the observed RMW distribution, similar to what is seen for high intensity storms (Hsu and Yan 1998).

Once we have calculated an RMW for each storm at each 15-minute time step, we can determine an associated radial profile of the azimuthal wind (Figure 4). Various parametric TC wind profile models exist (Chavas et al. 2015; Willoughby et al. 2006; Holland 1980); in all of them, azimuthal wind speed increases with radius from the eye of the storm until the RMW, at which value it begins to decrease with radius. We elect to use Willoughby et al. (2006), as it performs comparably well or slightly better than other wind profile models when compared to satellite-based observations of

hurricane wind fields (Yang et al. 2022). Inputs to this model are RMW, maximum sustained wind speed, and latitude, and the shape is determined by an empirically-fit double exponential profile.

The next step is to convert the one-dimensional radial profiles to two-dimensional wind swaths on a latitude-longitude grid. As we do this, we add a representation of asymmetry due to the translation of the storm along its track, which accelerates winds on the side of the storm where the rotating flow around the storm is in the same direction of the track, and decelerates them on the opposite side (Klotz and Jiang 2017; Uhlhorn et al. 2014). We first construct a $0.1°\times0.1°$ rectilinear grid spanning the Philippines. We then determine the track translation speed (V) and track direction (Θ) from a forward difference of the time step of interest and the subsequent time step. The azimuthal velocity at each grid point imposed by the translation of the storm can then be calculated as follows:

$$\begin{aligned} \theta_{i,j} &= \arctan2((y_{i,j}-Y),(x_{i,j}-X))-\Theta \\ v_{t(i,j)} &= -V*\cos(\pi/2-\theta_{i,j}), \end{aligned}$$

where X and Y are the longitude and latitude locations of the storm center, x and y are the longitude and latitude values for each point (i,j) on the grid, θ is the angle relative to the track direction at each location (i,j) on the grid, and v_t is the imposed tangential velocity from the storm translation at each point (i,j) on the grid.

Applying a large asymmetry correction far from the storm center can result in winds increasing with radius in some directions, a feature we view as unrealistic. Thus, we modulate v_t based on distance from the storm center before applying it to the wind field:

$$\begin{aligned} \alpha_{i,j}[r_{i,j}\geq 1] &= e^{-0.314-0.042r_{i,j}} \\ \alpha_{i,j}[r_{i,j}<1] &= 0.3r_{i,j}+0.4 \\ v_{a(i,j)} &= \alpha_{i,j}*v_{t(i,j)}, \end{aligned}$$

where r is the radius from the center of the storm in kilometers normalized by the RMW (so $r = 1$ at the RMW), and α is the factor modulating the asymmetry correction, and v_a is the asymmetry correction. α is designed assuming that the impact of the storm motion on the symmetric background wind is reduced with radius. The above equation gives us maximum asymmetries imposed by translation speed at the RMW with $\alpha = 0.7$ that gradually decrease to 0.3 outward. The values of α are within a rough range of the estimated values of storm translation to surface background wind reduction factor shown in Lin and Chavas (2012).

The final wind field is determined by re-gridding the Willoughby et al. (2006) radial wind profile to the latitude-longitude grid and adding the asymmetry correction ($v_{a(i,j)}$). To this end, to ensure the maximum wind speed remains unchanged, we input to the wind profile calculation the maximum sustained wind speed minus the maximum asymmetry correction ($\max(v_a) = 0.7 * \max(v_t)$). Once a wind field is determined for each 15-minute time step of a given storm, the final wind swath to be used in loss calculations is obtained by taking the maximum of all the wind fields across time at each latitude-longitude grid point. Examples of resulting wind swaths for nine of the most destructive historical storms in the Philippines are shown in Figure 4.

Here we presented a relatively simple construction of two-dimensional wind swaths that captures storm wind at first-order, and allows efficient generation of wind maps for large numbers of synthetic storms. However, there are a variety of ways in which this construction could be improved. For example, one can use a more sophisticated method in estimating RMW (Chavas and Knaff 2022) and in adding in asymmetries (Lin and Chavas 2012; Chang et al. 2020; Yang et al. 2022). Additionally, following landfall, another significant source of asymmetry in the wind field is the roughness of the land surface (e.g. from buildings, plants, and topography), which generally decelerates wind speeds. For our initial model described here, we neglect this roughness effect. This will lead to overestimates of the wind over land, but we view this as an acceptable compromise for the level

of analysis we conduct here, particularly because the vulnerability curves are calibrated to these winds. Roughness will be incorporated in future versions of the model.

b. Exposure

We represent exposure via a global dataset of assets in USD across space developed by Eberenz et al. (2020b). This dataset, called LitPop, is constructed by disaggregating 2014 national total asset value across space proportionally to population density and nightlights data. The national total asset value data used is the World Bank's produced capital stock, which represents the value of manufactured or built assets in each country, not including the value of agricultural products (World Bank 2021). The nightlights data used is NASA's Black Marble nighttime lights (Román et al. 2018), and the population data used is the Gridded Population of the World (Doxsey-Whitfield et al. 2015). Validating by disaggregating national GDP and comparing to regional GDP estimates in 14 countries, Eberenz et al. (2020b) finds that disaggregating proportionally to $Lit^1 Pop^1$ (where Lit is the nightlights data and Pop is the population data) likely provides the best estimate of asset distribution. It is worth noting that the validation exercise was performed in a set of 14 countries that did not include the Philippines. An improved Philippines-specific dataset might be constructed by fitting this dataset for the Philippines, and perhaps considering the distribution of agricultural products across space. But we expect that the existing dataset provides a reasonable enough estimate of asset distribution for this initial risk model. In the Philippines, LitPop shows by far the highest asset density in and around Manila, with more minor hot spots of asset concentration in other major cities (Figure 5).

LitPop is available at a relatively high 30 arcsec resolution, which is equivalent to the resolution of the underlying population data. To allow the wind hazard to interact with exposure, we bilinearly

interpolate the $0.1^\circ \times 0.1^\circ$ wind swaths to the higher resolution of the LitPop data. This is done to leverage the spatial detail in the exposure dataset.

c. Vulnerability

Vulnerability is the propensity of exposed value to be destroyed in the face of a geophysical hazard. In the context of our model, vulnerability converts a given wind speed to percentage of assets destroyed. Intuitively, at low to moderate wind speeds — i.e., those that are commonly experienced in the absence of a tropical cyclone — no damages should occur, and at high wind speeds damages should increase until they saturate at 100% of exposed value. There are a few different functional forms for TC wind-related vulnerability (called impact functions, vulnerability curves, or damage functions) that have been proposed. Here we use the functional form presented in Emanuel (2011), which is structured as follows:

$$f = \frac{v_n^3}{1+v_n^3} \tag{1}$$

$$v_n = \frac{\max[(V - V_{thresh}), 0]}{V_{half} - V_{thresh},} \tag{2}$$

where f is the fraction of the asset value lost, V is the wind speed, V_{thresh} is the wind speed at and below which no damage occurs, and V_{half} is the wind speed at which half the asset value is lost (Figure 6). The third power of wind speed in Equation 1 is based on physical arguments (Emanuel 2005) and empirical analysis, i.e. regression against historical losses in the USA (Strobl 2011). In the function shown in Equation 2, the parameters V_{thresh} and V_{half} determine vulnerability—lower values of these parameters correspond to higher vulnerability. V_{thresh} is necessarily always lower than V_{half}.

The vulnerability function above was developed to represent damage from extreme wind, but has been used to predict total TC-related damages in various applications. Most relevant to this

study, Eberenz et al. (2020a) (hereafter, “ELB21") fit country-wide impact functions to simulate total historical TC damages in different countries, including the Philippines. In this study, the values of V_{half} are varied to optimally simulate total damages, while V_{thresh} is kept constant at $25.7ms^{-1}$ ($50kts$), an approach that has been used and to some degree supported in other studies. For example, in Emanuel (2011) this $25.7ms^{-1}$ V_{thresh} value was proposed for the USA, while the value of V_{half} varied in order to represent different vulnerability levels, and this same V_{thresh} value is somewhat consistent with structural vulnerability curves for wind used in the Hazus risk modeling framework (Vickery et al. 2006b). This approach of varying V_{half} but not V_{thresh} has also been shown to reasonably simulate losses in China (Elliott et al. 2015). Since there is rather limited justification of this V_{thresh} value when using wind as a proxy for all damages, and it is plausible that lower V_{thresh} values may be justified to the extent that non-wind hazards (such as flooding) are being implicitly represented, we examine sensitivity of our risk results to both V_{half} and V_{thresh}.

Our process for fitting this vulnerability function for the Philippines is discussed in more detail in Section 3. A dataset we use in this fitting process is the Family Income and Expenditure Survey (FIES) for the Philippines. FIES is conducted by the Filipino government’s National Statistics Office, and is a key tool for poverty quantification (Ericta and Fabian 2009). It surveys tens of thousands of households in the Philippines on diverse and detailed aspects of their incomes, spending, and saving. Particularly relevant here, it also includes information on their dwellings. This survey is completed every three years. We employ 2015 data on dwelling construction materials (Bersales 2017). The FIES categorizes roof and wall construction materials into seven different categories, which can roughly be ordered from weakest to strongest. As discussed below, we employ this data as a proxy for TC structural vulnerability.

d. Reported Damage Data

To develop and validate our risk model, we compare our results to estimates of historical losses from real TCs that have affected the Philippines. For this purpose, we use the EM-DAT database, which aggregates data on a wide range of disasters (Guha-Sapir et al.). EM-DAT includes disasters from 1900 to the present that meet one of the following criteria: 10 or more people dead, 100 or more people affected, the declaration of a state of emergency, and/or a call for international assistance. Sources of data included in EM-DAT vary, but priority is given to information from UN agencies, governments, and the International Federation of Red Cross and Red Crescent Societies. From EM-DAT, we select only data entries for storms affecting the Philippines, and make use of the start date, end date, and total damages (in USD) for each storm. We retain storms that have damage estimates, start and end dates, and are not labelled as convective or extra-tropical events (260 events total). While tropical cyclones are convective in nature, all events with the convective label in Philippines EM-DAT are either tornados or related to frontal systems, hence their exclusion from our analysis. 245 of the 260 included events are labeled as TCs. The event names of the remaining 15 indicate that these are tropical depressions or tropical storms— we also include these in our analysis, as they were TCs but just did not have typhoon-intensity at the time of landfall in the Philippines. The timing of these events spans 1952 to the present (Figure 7). Their associated losses span many orders of magnitude, with the smallest loss for an individual TC event being 5000 USD, and the greatest loss being 10 billion USD, caused by Typhoon Haiyan.

The number of events included in the dataset also increases over time— this may result from changes in observing practices or actual increases in TC risk caused by population growth and development and/or changes in TC characteristics (in particular TC intensity) due to anthropogenic climate change (Knutson et al. 2020). Here, we evaluate the model by comparing simulated

damages to those in EM-DAT event-by-event, without explicitly considering when each event occurred, so any changes in observing practices are effectively random errors for our purpose. The possible effects of such changes would have to be considered more explicitly if one wished to study temporal trends in damage.

e. Comparison between Reported and Simulated Damages

To reasonably compare EM-DAT with our simulated damages we need to account for change in assets over time and inflation. However, the LitPop dataset uses asset data from 2014, while the damage values in EM-DAT should be compared to asset values at the time the event occurred. Therefore, in order to reasonably compare simulated and observed damages, we first normalize the observed damages to 2014 values via the Penn World Tables' (version 10.0) quantification of Philippines capital stock, which is closely related to total asset value (Feenstra et al. 2015) and provided in units of constant 2017 national prices in USD. Specifically, we follow a procedure similar to that in ELB21:

$$\mathrm{NRD}_E = \mathrm{RD}_E \frac{\mathrm{CS}_{2014}}{\mathrm{CS}_\mathrm{y}},$$

where E represents a particular event, y is the year the event occurs, RD is the raw reported damages, NRD is normalized reported damages, and CS is capital stock. For the rest of this paper, "reported damages" refers to damages normalized this way.

EM-DAT presents damages in entire country totals. For some events, additional information is provided specifying the region affected, but the lack of consistency in this information makes it difficult to employ in our analysis. As such, in validating simulated damages against reported damages, we always first sum all simulated damages across the Philippines.

To match reported damages with corresponding simulated damages, we employ the dates of the events from EM-DAT and IBTrACS. Since multiple storms can share some dates of occurrence, we match a reported damage entry and simulated damages when the number of days of overlap is maximized compared to any other possible matches. Using this method results in 134 unambiguous matches. There were some ambiguous matches that required special considerations. First, two sets of events share very similar dates—1995's typhoons Angela (Pepang) and Zack (Rosing), and 2016's typhoons Sarika (Karen) and Haima (Laiwin), where the first name is given by the Japan Meteorological Agency (JMA) and the second in parentheses is given locally by the Philippine Atmospheric, Geophysical, and Astronomical Services Administration (PAGASA), only when storms enter into their area of responsibility. For these pairs of TCs, matching was reconciled via looking up additional information about storm path and precise landfall date. There is also ambiguity for Typhoon Faye (Norming) in 1982 — two entries exist in EM-DAT for this event (one under Typhoon Faye, the name given by JMA, and one under Typhoon Norming, the local name given by PAGASA). These two entries have different damage estimates which appear to correspond to different landfalls of this one storm. We add these two damage estimates together to create one reported estimate for the typhoon that is comparable to the entire simulated event. Many storms are excluded because there is an IBTrACS track but no overlapping EM-DAT damage event, or vice versa. Altogether, this process results in matches for 139 events.

We use a few different metrics to compare reported and simulated damages. Three are standard metrics of correlation: Pearson's r, Kendall's τ, and Spearman's r. Pearson's r measures the linear correlation between two datasets, whereas Kendall's τ and Spearman's r are both non-parametric, rank-based correlation coefficients— they assess the extent to which one dataset is a monotonic function of the other. For all three of these metrics, model performance is better when the correlation is closer to 1. The two additional metrics are drawn from ELB21, and reflect

distinct needs in developing a TC risk model. The first metric is the total damage ratio (TDR), and is quantified as:

$$\mathrm{TDR} = \frac{\sum_{E=1}^{N} \mathrm{SD}_E}{\sum_{E=1}^{N} \mathrm{NRD}_E},$$

where E from 1 to N spans all the relevant historical TC events, NRD is the normalized reported damages, and SD is our model's simulated damages. A TDR of 1 is optimal. TDR reflects the ability of our risk model to simulate total damages across all events, and is dominated by the events that cause the greatest asset losses (e.g., Haiyan). However, as discussed further in Section 3, lack of skill in simulating more moderate events can be masked by TDR. To better assess skill across a range of events, ELB21 also introduces a metric called root-mean-squared fraction (RMSF), which is quantified as:

$$\mathrm{RMSF} = \exp\left(\sqrt{\frac{1}{N}\sum_{E=1}^{N}[\ln(\mathrm{EDR}_E)]^2}\right),$$

where EDR stands for "event damage ratio" and is defined as $\mathrm{SD}_E/\mathrm{NRD}_E$ for any given event. RMSF weighs errors proportionally to event magnitude, so that a 50% error (for example) is equally important whether it is 50% of a small loss or a large one. Values of RMSF closer to one represent lower model errors. TDR and RMSF reflect different considerations relevant to development of a TC risk model. Ideally a model would perform well for both metrics, but in general (and in our results below) there are trade-offs such that prioritizing one versus the other implies different modeling choices.

3. Development of the Vulnerability Layer

In this section, we estimate vulnerability across space in the Philippines, which we call a "vulnerability layer" to be combined with hazard and exposure to estimate Philippines TC risk. In developing a vulnerability layer, our general approach is to determine which vulnerability parameter values result in the best match between reported damages and simulated damages for historical TCs. As mentioned above, we only consider TCs that make landfall in the Philippines (excluding near misses), and are included in EM-DAT. Fitting vulnerability to damages as described here is primarily an empirical approach, though we note that the Emanuel (2011) vulnerability curve functional form we employ is also informed by the physics of wind-driven damage. Below we describe a couple of specific methods for fitting vulnerability in the Philippines with varying levels of spatial complexity.

a. National Fit

We initially apply the same vulnerability curve for all locations in the Philippines. This is similar to the approach employed in ELB21, who notably found very different values for V_{half} in the Philippines depending on whether TDR or RMSF was optimized, which were $85.7 ms^{-1}$ and $188.4 ms^{-1}$ respectively. Using these V_{half} values and the V_{thresh} value used in ELB21 ($25.7 ms^{-1}$) as a starting point, we test the sensitivity of simulated damages to V_{half} and V_{thresh}. Specifically, we evaluate simulated damages for V_{half} every $10 ms^{-1}$ between 50 and 200 ms^{-1}, and for V_{thresh} every $5 ms^{-1}$ between 15 and 35 ms^{-1}. For each combination of these parameter values, we calculate the various correlation metrics described in Section 2 comparing simulated versus reported damages (Figure 8). In this analysis, the parameter values for vulnerability are deemed more optimal when Pearson's r, Kendall's τ, and Spearman's r are closer to 1, TDR is closer to 1 (equivalent to ln(TDR) closer to 0), and RMSF is minimized.

This sensitivity analysis highlights the difficulty of confidently fitting a single vulnerability curve for the Philippines. Depending on the correlation metric examined, very different parameter values are found to be optimal. Not only that, but the structure of the dependence of the correlation metrics on the vulnerability parameters varies substantially. Pearson r is optimized for the highest values of V_{half} and V_{thresh}. Kendall τ and Spearman r, which are both rank-based, non-parametric correlation metrics, exhibit the strongest dependence on V_{thresh}, and are optimized for V_{thresh} equal to $30ms^{-1}$. TDR is optimized along a diagonal from high values of V_{thresh} and low values of V_{half} to low values of V_{thresh} and high values of V_{half}. Finally, RMSF is generally optimized for somewhat lower values of both parameters, and favors $V_{thresh]}$ equal to $20ms^{-1}$.

For TDR and RMSF, the results of our analysis are qualitatively similar to those of ELB21, though quantitatively different. If we hold V_{thresh} constant at $25ms^{-1}$, as ELB21 does, we find TDR is optimized at V_{half} equal to $150ms^{-1}$ and RMSF is optimized at V_{half} equal to $80ms^{-1}$. These values are both lower than the analogous fits in ELB21 ($188.4ms^{-1}$ and $84.7ms^{-1}$, respectively). This difference could perhaps be a consequence of ELB21 excluding storms where reported damages are positive but simulated damages are zero from their analysis, whereas we include such storms. However, additional differences may lie in the time span of the TC and damage data used, the wind field modeling, and the method of matching simulated damages and reported damages.

For the rest of the paper, we simplify our vulnerability fitting procedure in a few ways for parsimony and consistency with prior work. First, we focus on optimizing TDR and RMSF, which we believe are more intuitive to interpret than the other correlation metrics for emergency planning and preparedness. Second, rather than continuing to fit V_{thresh} and V_{half}, we hold V_{thresh} constant at $25ms^{-1}$ (same value as ELB21) and vary only V_{half}. As measured by TDR and RMSF, the degree of agreement with observed damages can be fit to some extent either by V_{thresh} or V_{half} (Figure 8d,e); focusing on V_{half} seems a reasonable simplifying assumption, especially as we have

a somewhat stronger *a priori* constraint on V_{thresh} (that is, that it should be somewhere near the low end of the maximum sustained wind speeds found in tropical storms). However, we emphasize that the sensitivity analysis shown in Figure 8 cannot clearly exclude values of V_{thresh} greater or lower than $25ms^{-1}$. Unlike prior work which has stated that V_{thresh} is relatively well-constrained to be around $25ms^{-1}$ (Emanuel 2011; Elliott et al. 2015), our analysis suggests further examination of appropriate V_{thresh} values is warranted, particularly in contexts where, as here, wind is being used as a proxy for all damages, rather than modeling only damages directly caused by wind.

Figure 9 plots reported against simulated damages for historical TCs, with the vulnerability parameter set to the optimal RMSF fit when holding V_{thresh} constant at $25ms^{-1}$ ($V_{half} = 80ms^{-1}$). When RMSF is minimized, TDR is 9.28— meaning total simulated damages are about 9× greater than those reported. This suggests a significant trade-off between capturing the damages for individual storms and across all storms when applying one vulnerability curve for the entire Philippines. To better understand the cause of this overestimation of total damages, we assessed possible commonalities among outliers. We found that storms passing through the large urban capital region, including Manila, by and large exhibited overestimated simulated damages. This is shown in Figure 9a by the blue circled values climbing the y-axis (simulated damages) for very low reported damages values, in Figure 9b by all the blue circled values lying above the black one-to-one line, and in Figure 9c by storms that pass through Manila disproportionately exhibiting high event damage ratios. Figure 9c is very similar to and inspired by Figure 7 in ELB21, though we find more storms with event damage ratios less than 0.1 as we include storms where simulated damages are 0.

These results seem to reflect the limitations of country-scale vulnerability in capturing significant urban-rural differences. Manila is much more built-up and wealthier than other regions in the Philippines, with likelier lower vulnerability (though greater exposure). As a result, when a

vulnerability curve fit for the entire Philippines is employed to calculate damages for a storm passing through Manila, damages are overestimated. Our hypothesis is that developing a more spatially detailed map of vulnerability in the Philippines would better capture these urban-rural differences, and allow more accurate simulation of damages for individual storms (i.e. lower RMSF) and across all storms (i.e. TDR closer to 1).

b. Regional Fit

Motivated by the results above, we develop a vulnerability layer with spatial variability in the vulnerability parameters. To capture a very high level of spatial detail, one might match buildings across the Philippines with building-type specific vulnerability curves similar to the methodology used for the US in FEMA's Hazus (Vickery et al. 2006b). However, this approach requires a detailed map of building types across the Philippines, which we lack. Instead, we take an intermediate approach between a single empirically-derived vulnerability curve for all the Philippines (the approach used in the previous section) and a building-level map of structural vulnerability to develop a region-scale TC vulnerability layer for the Philippines.

Our first step is to fit V_{half} for each region in the Philippines that has historically been damaged by TCs. A challenge here is that EM-DAT only provides nationally aggregated damage estimates. In lieu of region-level damage data, we fit V_{half} for each region based on the subset of historical storms that result in positive simulated asset losses for that region. Given the limitations of EM-DAT we also compare the national sum of reported damages to simulated damages, but just for the subset of storms affecting a given region. The assumption here is that even though the damage estimate for any given storm may be affected by neighboring regions impacted by the same TC, in aggregate across all historical storms this subset should reflect the TC risk for the region of interest. We then determine the V_{half} values that minimize RMSF for storms affecting each region. For

most regions, V_{half} ranges from $60 - 120 ms^{-1}$. Manila, as predicted, exhibits lower vulnerability than any other region, with an optimal V_{half} equal to $180 ms^{-1}$.

Because some regions of the Philippines have been affected by very few storms in the historical record, however, it is highly uncertain or impossible to fit V_{half} using the method described above for every region. For example, the Autonomous Region in Muslim Mindanao (ARMM) has experienced zero recorded landfalling storms according to our analysis of IBTrACS. To create a vulnerability map that is consistent across the Philippines, and also lend further confidence to our vulnerability quantification, we employ on-the-ground data about structural vulnerability included in the FIES. The FIES surveys a sample of households and groups them by region, making it possible to derive region-scale information. While the FIES includes information on both roof and wall construction materials, we focus on the roof materials, as most TC structural damage occurs through damage to the roof allowing rain to enter a building (Rowe 2021). The roof materials listed in the FIES dataset fall into seven categories (Figure 10). Most roofs are categorized as "strong material (galvanized, iron, al[uminum], tile, concrete, brick, stone, asbestos)" or "light material (cogon, nipa, anahaw)". Cogon, nipa, and anahaw are plant materials used to make straw thatch roofs. We use the ratio of strong to light roof materials as a proxy for structural vulnerability (Figure 11). As might be expected, the region of Manila has the highest proportion of strong to light roofs, whereas a more rural and impoverished region such as Eastern Visayas has a much lower proportion of strong to light roofs.

We hypothesize that the proportion of strong to light roofs influences TC vulnerability and should positively correlate with the V_{half} value fit in different regions. Indeed, we find a positive association between these two quantities (Figure 12a; NCR is the top-right point in the plot). This association likely reflects the direct impact of roof strength on TC damages, as well as other socioeconomic factors such as income and extent of the social safety net, which partially correlate

with construction quality and influence disaster outcomes. We linearly regress the proportion of strong to light roofs against V_{half}, and use the resulting regression coefficients and regional values of the roof proportion to calculate a final V_{half} value for each region (Figure 12a). The resulting map of vulnerability (represented by V_{half} values; Figure 12b) is similar to the map of socioeconomic resilience shown in Figure 1: vulnerability is higher in the south, and lower in the north, especially close to Manila.

We employ this map of regional vulnerability to recalculate simulated damages for historical storms making landfall in the Philippines and compare to reported damages from EM-DAT. The results of this analysis are shown in Figures 13 and 14. Compared to the nationally fit vulnerability curves minimizing RMSF (Figure 9), the regionally-varying vulnerability curves result in smaller RMSF (81 versus 92). Perhaps more striking, TDR is reduced from 9.28 to 2.02, even though TDR was not explicitly optimized for. For individual regions in the Philippines, TDR calculated for the subset of storms affecting each region is much improved as well. With a single national vulnerability curve, northern regions reach TDR values above 20 (Figure 14). In contrast, considering regionally varying vulnerability curves, leads to TDR values below 10 across the Philippines, and in most cases quite close to 1.

While key aspects of the simulated damages compare better to reported estimates with spatially varying vulnerability, as described above, others do not. In particular, with both versions of the vulnerability layer (national and regional) there are many storms with substantial reported damages that have zero simulated damages (Figure 13b). This error likely represents a structural limitation of our risk model. Here we use wind as a proxy for all TC-related damages. However, other hazards associated with TCs (storm surge, flooding due to rainfall, landslides) may occur at relatively low wind speeds (e.g. lower than the V_{thresh} value of $25 ms^{-1}$ used in the vulnerability curve), and result in damages which our model does not capture.

As an illustrative example, simulated damages from typhoons Haiyan (Yolanda) and Ketsana (Ondoy) are shown in Figure 15. Our model simulates no damages resulting from Ketsana, though it actually produced damages of 240 million USD according to EM-DAT. This appears to be because Ketsana was a relatively weak storm (tropical storm intensity) in terms of wind speed when it affected the Philippines, with damages dominated by extreme rainfall and flash flooding (Sato and Nakasu 2011), processes our model does not represent in any explicit way. In contrast, our model does simulate billions of USD worth of damages from Typhoon Haiyan, though it underestimates those damages by a factor of 5. This may reflect the lack of explicit storm surge in our model, as a large fraction of the damages caused by Haiyan resulted from storm surge (Lagmay et al. 2015).

4. Return Periods of TC Risk in the Philippines

The goal of this work was to create a usable, country and regional-scale TC risk model for the Philippines. Before concluding the paper, we briefly highlight the utility of our model for estimating TC risk return periods in the Philippines.

In assessing TC risk for diverse aspects of emergency preparedness, from building construction standards to emergency response plans, it is useful to know the expected frequency of events of a given severity. This is typically quantified as a return period (1/frequency) in units of years. Using our model, we can calculate return periods empirically for both wind speed and asset losses for different regions in the Philippines (examples for NCR and Eastern Visayas are shown in Figure 16). The most accurate hazard input is obtained using historical TC tracks, but this allows accurate estimation only at return periods several times shorter than the length of the historical record (76 years). Using our TC risk model run with CHAZ tracks allows consistent estimation of TC wind speed and asset losses out to much longer return periods. For CHAZ, we specify the duration used for frequency and return period calculation such that the regional landfall rate per year in CHAZ

is consistent with that of the historical record— i.e. for each region:

$$duration_{\mathrm{CHAZ}} = landfalls_{\mathrm{CHAZ}}/(landfalls_{\mathrm{IBTrACS}}/duration_{\mathrm{IBTrACS}}),$$

which amounts to a regional-scale bias correction on the landfall rate.

Both the advantages and the challenges of this approach are clearly demonstrated in determining the return period for a Haiyan-like event in Eastern Visayas as shown in Figure 16. Based on the historical record, in Eastern Visayas Typhoon Haiyan has a return period of about 70-80 years (since it occurred within the bounds of a historical record of approximately that length), but is clearly an outlier and not well-constrained. In the context of the much larger sample of physically plausible TCs from CHAZ, the hazard associated with a Haiyan-like event has a return period of several thousand years, and the losses from such an event are outside the range of synthetic storms (e.g. return period greater than 10,000 years). While the larger sample of storms may more robustly constrain the return period of this event, there are important caveats to consider with this estimate. In particular, CHAZ (like any model) may have biases— in Eastern Visayas, CHAZ-based asset losses appear to be biased somewhat too low given that the historical records lies slightly above the intensity ensemble (thin red lines). While we perform some light bias correction on the regional landfall rate (as mentioned in the prior paragraph), more intensive bias corrections could be applied, such as sub-selecting more realistic CHAZ tracks. Additionally, the CHAZ simulations here used environmental variables taken from the ERA-Interim Reanalysis in the recent historical period, with all years treated the same in the return period calculation; thus any possible climate change signal would be obscured to the extent that it might render 2013 (when Haiyan occurred) different than the earlier part of the period.

5. Summary & Conclusions

We have described the development and application of a TC risk model for the Philippines. This model includes three layers—hazard, exposure, and vulnerability— which, when combined, allow quantification of asset losses from storms. The present study focuses on the Philippines, but the methodology could be straightforwardly applied to other countries. Hazard is represented by swaths of maximum sustained wind speeds, derived from a parametric wind field model with a simple geometric correction for TC asymmetry. Swaths can be derived from observed TC tracks (e.g. IBTrACS) or synthetically generated TC tracks, such as from CHAZ. Exposure is the existing LitPop dataset, which distributes national total asset value across each country proportional to a combination of nightlights and population data (Eberenz et al. 2020b). For vulnerability, we employ the Emanuel (2011) functional form for vulnerability. However, we run a number of tests to fit the vulnerability curve parameters (V_{half}) to accurately simulate historical losses. This work is novel in two main ways. First, while there are other existing TC risk models, this is the first attempt to utilize the CHAZ model to quantify economic risks from TCs, opening the door for a variety of future applications. Second, we demonstrate the benefits of fitting regional (as opposed to national) vulnerability curves based on open-source economic data for TC risk analysis.

Initially, we tried fitting one vulnerability curve for the entire Philippines. Similar to results in ELB21, we find that this approach results in substantial uncertainty regarding the appropriate vulnerability curve. If the vulnerability is fit to best represent total damages (TDR close to 1), damages from TCs that pass through Manila are well simulated, while damages from other storms are underestimated. In contrast, if all storms are weighted equally in fitting vulnerability (RMSF minimized), damages from TCs that pass through Manila are substantially overestimated, and the TDR is approximately 9.

We hypothesized that this trade-off regarding the appropriate vulnerability curve resulted from urban-rural differences not captured by a national-scale vulnerability fit. We tried instead fitting V_{half} for each region to minimize RMSF based on the subset of historical storms that affected each region. The V_{half} values from this analysis suggest that Manila indeed has the lowest vulnerability in the Philippines. These parameter values were also found to be positively correlated with a proxy of structural vulnerability based on household survey data, namely, the proportion of strong to light roofs. Regressing V_{half} against this roof strength proportion, we determined V_{half} values for each region of the Philippines, and in so doing a regional map of TC vulnerability. Applying this regional TC vulnerability layer to simulate historical Philippines storms, we find lower RMSF, TDR across the Philippines of 2, and TDR values for individual provinces much closer to 1. We conclude that regional, and especially urban versus rural, differentiation of vulnerability is critical for accurate TC risk modeling in the Philippines.

We hope the initial TC risk model presented here may serve as a basis for further open-source TC risk modeling. Many aspects of this model could be improved, and we highlight a few here. On the hazard front, modeling of other TC-related hazards beyond wind could allow better simulation of impacts from many storms (Lin et al. 2010, 2012; Aerts et al. 2013; Rodrigo et al. 2018). At present, our model simulates zero damages for some historical TCs that did in fact produce damage. We believe this is because these are storms dominated by rainfall and flooding— hazards that are only indirectly, and very loosely, related to wind speed. Regarding the existing wind model, capturing surface roughness could allow more accurate simulation of wind speeds, and in turn damages, over land. We expect this limitation to be much less important than the omission of flooding, however, in part because our vulnerability curves are fit to the winds we use. The regional vulnerability approach can compensate further (compared to the national fit) for the lack of roughness in our model, as vulnerability is found to be lowest in urban regions where roughness would likely be

decelerating surface winds to the greatest extent. The method of incorporating TC asymmetry here is also a relatively simple function of TC translation, which might be superseded in future model iterations by more advanced methods (Lin and Chavas 2012; Chang et al. 2020; Yang et al. 2022).

There are many areas within the vulnerability and exposure modeling that merit further development as well. First, agricultural losses could be more rigorously quantified. At present, the exposure layer includes built assets, but does not explicitly include agriculture. This may bias our results, as agricultural losses have been significant in many historical Philippines TCs (Eberenz et al. 2020a). Second, appropriate values of the vulnerability parameter V_{thresh} might be more robustly determined, particularly in countries with a wide range of different construction standards. Here we have focused primarily on fitting V_{half}, but our national vulnerability curve fitting results suggests that in some circumstances values of V_{thresh} higher or lower than that used here ($25 ms^{-1}$, similar with prior work) could be more accurate. This issue is perhaps particularly acute when wind is used as a proxy for all TC-related hazards, since substantial flooding can occur at relatively small wind speeds. Third, more work could be done to examine the causes of the regional variation in vulnerability. While we relate regional V_{thresh} values to a measure of the strength of roof construction materials, the positive relationship between these two quantities does not necessarily reflect stronger roofs directly reducing vulnerability. Proportion of strong roofs may simply correlate with other quantities that could reduce vulnerability, such as wealth and urbanization. Indeed, in some small island communities in the Philippines, light cogon roofs are actually reported to be adaptive to tropical cyclones, as they can be tied down in high winds (Board 2019), highlighting a limitations of our focus on strong/heavy roofs to explain vulnerability. Fourth and finally, while moving from national to regional scale vulnerability significantly improved model accuracy, even higher resolution vulnerability layers (e.g. province or even building scale) may result in further improvements.

The current model quality encourages caution in interpreting results from such analyses, especially for individual storms which could be dominated by hazards other than wind. However, in simulating aggregate damages across many storms, the present risk model exhibits significant skill. Building on the return period analysis, we hope in future work to estimate projected changes in TC risk with global warming via pairing this model with CHAZ tracks generated using environmental variables taken from climate change scenarios simulated with earth system models (Emanuel 2011; Lee et al. 2020). Such results would be relevant to both adaptation planning and financial risk modeling, which regulations increasingly require to consider climate change (Fiedler et al. 2021).

Despite these various limitations, the model and analysis presented here generates insights useful for all stages of disaster risk management policy dialogues. Expected asset losses are used in sovereign risk financing dialogues to define needs and insurance premiums. Simulations of extreme events are useful for assessing tail risks and compound shocks, relevant to macro-fiscal and humanitarian contingency planning. We intend to extend this model to assess TC impacts across the income distribution, which is useful for mapping and addressing vulnerabilities, and for crafting post-disaster assistance packages. All of these considerations are in flux due to differential economic and population growth throughout the Philippines, and climate change. Because of these dynamics, perhaps the most salient contribution of this work to domestic policy and international development is its open source methods and code, which increase access to resources generally reserved for wealthy countries, the reinsurance industry, and private capital.

Acknowledgments. We would like to thank Samuel Eberenz, Olivia Cabrera, Dail Rowe, Kyle Mandli, and Stephane Hallegatte for useful conversations and feedback. We also thank Qidong Yang for sharing his implementation of the Willoughby wind profile model. JWB was supported by the Lamont-Doherty Earth Observatory Postdoctoral Fellowship. CYL and SJC thank support

from the Vetlesen Foundation to the Lamont-Doherty Earth Observatory of Columbia University. SJC, CYL, and AHS acknowledge support from the Swiss Re Foundation.

Data availability statement. Upon acceptance, code and data supporting the analyses and figures in this manuscript will be made publicly available through Github and public links to data servers. The Columbia tropical cyclone hazard model (CHAZ) is available on Github `https://github.com/cl3225/CHAZ`. LitPop is available online at `https://www.research-collection.ethz.ch/handle/20.500.11850/331316`. EM-DAT is available online at `https://public.emdat.be/`.

References

Aerts, J. C., N. Lin, W. Botzen, K. Emanuel, and H. de Moel, 2013: Low-probability flood risk modeling for New York City. *Risk Analysis*, **33 (5)**, 772–788, publisher: Wiley Online Library.

Bersales, L. G. S., 2017: 2015 Family Income and Expenditure Survey. Tech. rep., Philippine Statistics Authority. URL https://psa.gov.ph/sites/default/files/FIES%202015%20Final%20Report.pdf.

Beven, J. L., and Coauthors, 2008: Atlantic Hurricane Season of 2005. *Monthly Weather Review*, **136 (3)**, 1109–1173, doi:10.1175/2007MWR2074.1, URL https://journals.ametsoc.org/view/journals/mwre/136/3/2007mwr2074.1.xml, publisher: American Meteorological Society Section: Monthly Weather Review.

Bloemendaal, N., H. de Moel, S. Muis, I. D. Haigh, and J. C. J. H. Aerts, 2020a: Estimation of global tropical cyclone wind speed probabilities using the STORM dataset. *Scientific Data*, **7 (1)**, 377, doi:10.1038/s41597-020-00720-x, URL https://www.nature.com/articles/s41597-020-00720-x, number: 1 Publisher: Nature Publishing Group.

Bloemendaal, N., I. D. Haigh, H. de Moel, S. Muis, R. J. Haarsma, and J. C. J. H. Aerts, 2020b: Generation of a global synthetic tropical cyclone hazard dataset using STORM. *Scientific Data*, **7 (1)**, 40, doi:10.1038/s41597-020-0381-2, URL https://www.nature.com/articles/s41597-020-0381-2, number: 1 Publisher: Nature Publishing Group.

Board, J., 2019: In the path of the storm: Life in Batanes on the Philippines' typhoon track. *Channel News Asia*, URL https://www.channelnewsasia.com/asia/islands-in-the-path-of-typhoons-life-in-batanes-philippines-792076.

Chang, D., S. Amin, and K. Emanuel, 2020: Modeling and Parameter Estimation of Hurricane Wind Fields with Asymmetry. *Journal of Applied Meteorology and Climatology*, **59 (4)**, 687–705, doi:10.1175/JAMC-D-19-0126.1, URL https://journals.ametsoc.org/view/journals/apme/59/4/jamc-d-19-0126.1.xml, publisher: American Meteorological Society Section: Journal of Applied Meteorology and Climatology.

Chavas, D. R., and J. A. Knaff, 2022: A simple model for predicting the tropical cyclone radius of maximum wind from outer size. *Weather and Forecasting*, **- 1 (aop)**, doi:10.1175/WAF-D-21-0103.1, URL https://journals.ametsoc.org/view/journals/wefo/aop/WAF-D-21-0103.1/WAF-D-21-0103.1.xml, publisher: American Meteorological Society Section: Weather and Forecasting.

Chavas, D. R., N. Lin, and K. Emanuel, 2015: A Model for the Complete Radial Structure of the Tropical Cyclone Wind Field. Part I: Comparison with Observed Structure. *Journal of the Atmospheric Sciences*, **72 (9)**, 3647–3662, doi:10.1175/JAS-D-15-0014.1, URL https://journals.ametsoc.org/doi/full/10.1175/JAS-D-15-0014.1, publisher: American Meteorological Society.

Cinco, T. A., and Coauthors, 2016: Observed trends and impacts of tropical cyclones in the Philippines. *International Journal of Climatology*, **36 (14)**, 4638–4650,

doi:10.1002/joc.4659, URL https://onlinelibrary.wiley.com/doi/abs/10.1002/joc.4659, _eprint: https://onlinelibrary.wiley.com/doi/pdf/10.1002/joc.4659.

Corporal-Lodangco, I. L., and L. M. Leslie, 2017: Climatology of Philippine tropical cyclone activity: 1945–2011. *International Journal of Climatology*, **37 (9)**, 3525–3539, publisher: Wiley Online Library.

Corporal-Lodangco, I. L., L. M. Leslie, and P. J. Lamb, 2016: Impacts of ENSO on Philippine tropical cyclone activity. *Journal of Climate*, **29 (5)**, 1877–1897.

Cutter, S. L., B. J. Boruff, and W. L. Shirley, 2003: Social Vulnerability to Environmental Hazards*. *Social Science Quarterly*, **84 (2)**, 242–261, doi:https://doi.org/10.1111/1540-6237.8402002, URL https://onlinelibrary.wiley.com/doi/abs/10.1111/1540-6237.8402002, _eprint: https://onlinelibrary.wiley.com/doi/pdf/10.1111/1540-6237.8402002.

Dee, D. P., and Coauthors, 2011: The ERA-Interim reanalysis: Configuration and performance of the data assimilation system. *Quarterly Journal of the Royal Meteorological Society*, **137 (656)**, 553–597, URL http://onlinelibrary.wiley.com/doi/10.1002/qj.828/full.

del Rosario, E. D., ????: Final Report re Effects of Typhoon "Yolanda" (Haiyan). Tech. rep., National Disaster Risk Reduction and Management Council, Republic of the Philippines, Quezon City, Philippines, 148 pp. URL https://ndrrmc.gov.ph/attachments/article/1329/FINAL_REPORT_re_Effects_of_Typhoon_YOLANDA_(HAIYAN)_06-09NOV2013.pdf.

Deuchert, E., and C. Felfe, 2015: The tempest: Short-and long-term consequences of a natural disaster for children s development. *European Economic Review*, **80**, 280–294, publisher: Elsevier.

Dominguez, C., A. Jaramillo, and P. Cuéllar, 2021: Are the socioeconomic impacts associated with tropical cyclones in Mexico exacerbated by local vulnerability and ENSO conditions? *International Journal of Climatology*, **41 (S1)**, E3307–E3324, doi:10.1002/joc.6927, URL https://onlinelibrary.wiley.com/doi/abs/10.1002/joc.6927, _eprint: https://onlinelibrary.wiley.com/doi/pdf/10.1002/joc.6927.

Doxsey-Whitfield, E., K. MacManus, S. B. Adamo, L. Pistolesi, J. Squires, O. Borkovska, and S. R. Baptista, 2015: Taking advantage of the improved availability of census data: a first look at the gridded population of the world, version 4. *Papers in Applied Geography*, **1 (3)**, 226–234, publisher: Taylor & Francis.

Eadie, P., M. E. Atienza, and M. Tan-Mullins, 2020: Livelihood and vulnerability in the wake of Typhoon Yolanda: lessons of community and resilience. *Natural Hazards*, **103 (1)**.

Eberenz, S., S. Lüthi, and D. N. Bresch, 2020a: Regional tropical cyclone impact functions for globally consistent risk assessments. *Natural Hazards and Earth System Sciences Discussions*, 1–29, doi:https://doi.org/10.5194/nhess-2020-229, URL https://nhess.copernicus.org/preprints/nhess-2020-229/, publisher: Copernicus GmbH.

Eberenz, S., D. Stocker, T. Röösli, and D. N. Bresch, 2020b: Asset exposure data for global physical risk assessment. *Earth System Science Data*, **12 (2)**, 817–833, publisher: Copernicus Publication.

Ehrhart, B., S. Mildenhall, A. Podlaha, and S. Bowen, 2014: Annual Global Climate and Catastrophe Report: Impact Forecasting — 2013. Tech. rep., Aon Benfield. URL http://thoughtleadership.aon.com/Documents/20140113_ab_if_annual_climate_catastrophe_report.pdf.

Elliott, R. J. R., E. Strobl, and P. Sun, 2015: The local impact of typhoons on economic activity in China: A view from outer space. *Journal of Urban Economics*, **88**, 50–66, doi:10.1016/j.jue.2015.05.001, URL http://www.sciencedirect.com/science/article/pii/S0094119015000340.

Emanuel, K., 2005: Increasing destructiveness of tropical cyclones over the past 30 years. *Nature*, **436 (7051)**, 686–688, doi:10.1038/nature03906, URL https://www.nature.com/articles/nature03906, number: 7051 Publisher: Nature Publishing Group.

Emanuel, K., 2011: Global warming effects on US hurricane damage. *Weather, Climate, and Society*, **3 (4)**, 261–268.

Ericta, C. N., and E. Fabian, 2009: A Documentation of the Philippines' Family Income and Expenditure Survey. Working Paper 2009-18, PIDS Discussion Paper Series. URL https://www.econstor.eu/handle/10419/126778.

Feenstra, R. C., R. Inklaar, and M. P. Timmer, 2015: The next generation of the Penn World Table. *American economic review*, **105 (10)**, 3150–82.

Fiedler, T., A. J. Pitman, K. Mackenzie, N. Wood, C. Jakob, and S. E. Perkins-Kirkpatrick, 2021: Business risk and the emergence of climate analytics. *Nature Climate Change*, **11 (2)**, 87–94, doi:10.1038/s41558-020-00984-6, URL https://www.nature.com/articles/s41558-020-00984-6, number: 2 Publisher: Nature Publishing Group.

Field, C. B., and Coauthors, 2012: *Managing the Risks of Extreme Events and Disasters to Advance Climate Change Adaptation. A Special Report of Working Groups I and II of IPCC Intergovernmental Panel on Climate Change*. Cambridge University Press, Cambridge, URL https://boris.unibe.ch/71442/.

Gori, A., N. Lin, D. Xi, and K. Emanuel, 2022: Tropical cyclone climatology change greatly exacerbates US extreme rainfall–surge hazard. *Nature Climate Change*, 1–8, doi:10.1038/s41558-021-01272-7, URL https://www.nature.com/articles/s41558-021-01272-7, publisher: Nature Publishing Group.

Guha-Sapir, D., R. Below, and P. Hoyois, ????: EM-DAT: The CRED/OFDA International Disaster Database. Tech. rep., Université Catholique de Louvain, Brussels, Belgium. URL www.emdat.be.

Hallegatte, S., A. Vogt-Schilb, M. Bangalore, and J. Rozenberg, 2016: *Unbreakable: building the resilience of the poor in the face of natural disasters*. World Bank Publications.

Holland, G. J., 1980: An analytic model of the wind and pressure profiles in hurricanes. *Monthly weather review*, **108 (8)**, 1212–1218.

Hsu, S. A., and Z. Yan, 1998: A note on the radius of maximum wind for hurricanes. *Journal of coastal research*, **14 (2)**.

Jing, R., and N. Lin, 2020: An Environment-Dependent Probabilistic Tropical Cyclone Model. *Journal of Advances in Modeling Earth Systems*, **12 (3)**, e2019MS001 975, doi:https://doi.org/10.1029/2019MS001975, URL https://agupubs.onlinelibrary.wiley.com/doi/abs/10.1029/2019MS001975, _eprint: https://agupubs.onlinelibrary.wiley.com/doi/pdf/10.1029/2019MS001975.

Klotz, B. W., and H. Jiang, 2017: Examination of surface wind asymmetries in tropical cyclones. Part I: General structure and wind shear impacts. *Monthly Weather Review*, **145 (10)**, 3989–4009, publisher: American Meteorological Society.

Knaff, J. A., S. P. Longmore, R. T. DeMaria, and D. A. Molenar, 2015: Improved Tropical-Cyclone Flight-Level Wind Estimates Using Routine Infrared Satellite Recon-

naissance. *Journal of Applied Meteorology and Climatology*, **54 (2)**, 463–478, doi: 10.1175/JAMC-D-14-0112.1, URL https://journals.ametsoc.org/jamc/article/54/2/463/13954/ Improved-Tropical-Cyclone-Flight-Level-Wind, publisher: American Meteorological Society.

Knapp, K. R., M. C. Kruk, D. H. Levinson, H. J. Diamond, and C. J. Neumann, 2010: The international best track archive for climate stewardship (IBTrACS) unifying tropical cyclone data. *Bulletin of the American Meteorological Society*, **91 (3)**, 363–376, publisher: American Meteorological Society.

Knutson, T., and Coauthors, 2020: Tropical cyclones and climate change assessment: Part II: Projected response to anthropogenic warming. *Bulletin of the American Meteorological Society*, **101 (3)**, E303–E322, publisher: American Meteorological Society.

Lagmay, A. M. F., and Coauthors, 2015: Devastating storm surges of Typhoon Haiyan. *International Journal of Disaster Risk Reduction*, **11**, 1–12, doi:10.1016/j.ijdrr.2014.10.006, URL https://www.sciencedirect.com/science/article/pii/S2212420914000922.

Lee, C.-Y., S. J. Camargo, A. H. Sobel, and M. K. Tippett, 2020: Statistical–dynamical downscaling projections of tropical cyclone activity in a warming climate: Two diverging genesis scenarios. *Journal of Climate*, **33 (11)**, 4815–4834.

Lee, C.-Y., M. K. Tippett, A. H. Sobel, and S. J. Camargo, 2016: Autoregressive Modeling for Tropical Cyclone Intensity Climatology. *Journal of Climate*, **29 (21)**, 7815–7830, doi:10.1175/JCLI-D-15-0909.1, URL https://journals.ametsoc.org/view/journals/clim/29/21/ jcli-d-15-0909.1.xml, publisher: American Meteorological Society Section: Journal of Climate.

Lee, C.-Y., M. K. Tippett, A. H. Sobel, and S. J. Camargo, 2018: An Environmentally Forced Tropical Cyclone Hazard Model. *Journal of Advances in Modeling Earth Systems*, **10 (1)**, 223–241, doi:https://doi.org/10.1002/2017MS001186, URL https://agupubs.onlinelibrary.wiley.com/doi/abs/10.1002/2017MS001186, _eprint: https://agupubs.onlinelibrary.wiley.com/doi/pdf/10.1002/2017MS001186.

Leonard, M., and Coauthors, 2014: A compound event framework for understanding extreme impacts. *Wiley Interdisciplinary Reviews: Climate Change*, **5 (1)**, 113–128, doi:10.1002/wcc.252, URL http://onlinelibrary.wiley.com/doi/10.1002/wcc.252/abstract.

Lin, I.-I., I.-F. Pun, and C.-C. Lien, 2014: "Category-6" supertyphoon Haiyan in global warming hiatus: Contribution from subsurface ocean warming. *Geophysical Research Letters*, **41 (23)**, 8547–8553, publisher: Wiley Online Library.

Lin, N., and D. Chavas, 2012: On hurricane parametric wind and applications in storm surge modeling. *Journal of Geophysical Research: Atmospheres*, **117 (D9)**, doi:https://doi.org/10.1029/2011JD017126, URL https://agupubs.onlinelibrary.wiley.com/doi/abs/10.1029/2011JD017126, _eprint: https://agupubs.onlinelibrary.wiley.com/doi/pdf/10.1029/2011JD017126.

Lin, N., K. Emanuel, M. Oppenheimer, and E. Vanmarcke, 2012: Physically based assessment of hurricane surge threat under climate change. *Nature Climate Change*, **2 (6)**, 462–467, doi:10.1038/nclimate1389, URL https://www.nature.com/articles/nclimate1389, number: 6 Publisher: Nature Publishing Group.

Lin, N., K. A. Emanuel, J. A. Smith, and E. Vanmarcke, 2010: Risk assessment of hurricane storm surge for New York City. *Journal of Geophysical Research: Atmospheres*, **115 (D18)**, publisher: Wiley Online Library.

Lyon, B., and S. J. Camargo, 2009: The seasonally-varying influence of ENSO on rainfall and tropical cyclone activity in the Philippines. *Climate Dynamics*, **32 (1)**, 125–141, doi:10.1007/s00382-008-0380-z, URL https://doi.org/10.1007/s00382-008-0380-z.

Mas, E., J. Bricker, S. Kure, B. Adriano, C. Yi, A. Suppasri, and S. Koshimura, 2015: Field survey report and satellite image interpretation of the 2013 Super Typhoon Haiyan in the Philippines. *Natural Hazards and Earth System Sciences*, **15 (4)**, 805–816, publisher: Copernicus GmbH.

Matthews, T., R. L. Wilby, and C. Murphy, 2019: An emerging tropical cyclone–deadly heat compound hazard. *Nature Climate Change*, **9 (8)**, 602–606, doi:10.1038/s41558-019-0525-6, URL https://www.nature.com/articles/s41558-019-0525-6.

Meiler, S., T. Vogt, N. Bloemendaal, A. Ciullo, C.-Y. Lee, S. Camargo, K. Emanuel, and D. Bresch, 2022: Intercomparison of regional loss estimates from global synthetic tropical cyclone models. Tech. rep. doi:10.21203/rs.3.rs-1429968/v1, URL https://www.researchsquare.com/article/rs-1429968/v1, iSSN: 2693-5015 Type: article.

Noy, I., 2009: The macroeconomic consequences of disasters. *Journal of Development economics*, **88 (2)**, 221–231, publisher: Elsevier.

OCHA, 2022: Philippines: Super Typhoon Rai (Odette). Tech. Rep. 7, United Nations. URL https://reliefweb.int/report/philippines/philippines-super-typhoon-rai-odette-situation-report-no-7-25-march-2022.

Ribera, P., R. García Herrera, and L. Gimeno, 2008: Historical deadly typhoons in the Philippines. *Weather*, **63 (7)**, 194, publisher: John Wiley & Sons LTD.

Rodrigo, S. M. T., C. L. Villanoy, J. C. Briones, P. H. T. Bilgera, O. C. Cabrera, and G. T. T. Narisma, 2018: The mapping of storm surge-prone areas and characterizing surge-producing cyclones in

Leyte Gulf, Philippines. *Natural Hazards*, **92 (3)**, 1305–1320, doi:10.1007/s11069-018-3252-9, URL https://doi.org/10.1007/s11069-018-3252-9.

Román, M. O., and Coauthors, 2018: NASA's Black Marble nighttime lights product suite. *Remote Sensing of Environment*, **210**, 113–143, publisher: Elsevier.

Rowe, D., 2021: Personal communication.

Sakai, Y., J. P. Estudillo, N. Fuwa, Y. Higuchi, and Y. Sawada, 2017: Do natural disasters affect the poor disproportionately? Price change and welfare impact in the aftermath of Typhoon Milenyo in the rural Philippines. *World Development*, **94**, 16–26, publisher: Elsevier.

Sato, T., and T. Nakasu, 2011: 2009 Typhoon Ondoy Flood Disasters in Metro Manila. *Natural Disaster Research Report*, **45**, 63–74.

Sobel, A. H., C.-Y. Lee, S. J. Camargo, K. T. Mandli, K. A. Emanuel, P. Mukhopadhyay, and M. Mahakur, 2019: Tropical cyclone hazard to Mumbai in the recent historical climate. *Monthly Weather Review*, **147 (7)**, 2355–2366.

Soria, J. L. A., and Coauthors, 2016: Repeat storm surge disasters of Typhoon Haiyan and its 1897 predecessor in the Philippines. *Bulletin of the American Meteorological Society*, **97 (1)**, 31–48, publisher: American Meteorological Society.

Strobl, E., 2011: The Economic Growth Impact of Hurricanes: Evidence from U.S. Coastal Counties. *The Review of Economics and Statistics*, **93 (2)**, 575–589, URL https://econpapers.repec.org/article/tprrestat/v_3a93_3ay_3a2011_3ai_3a2_3ap_3a575-589.htm, publisher: MIT Press.

Tellman, B., C. Schank, B. Schwarz, P. D. Howe, and A. de Sherbinin, 2020: Using Disaster Outcomes to Validate Components of Social Vulnerability to Floods: Flood Deaths and Prop-

erty Damage across the USA. *Sustainability*, **12 (15)**, 6006, doi:10.3390/su12156006, URL https://www.mdpi.com/2071-1050/12/15/6006, number: 15 Publisher: Multidisciplinary Digital Publishing Institute.

Uhlhorn, E. W., B. W. Klotz, T. Vukicevic, P. D. Reasor, and R. F. Rogers, 2014: Observed Hurricane Wind Speed Asymmetries and Relationships to Motion and Environmental Shear. *Monthly Weather Review*, **142 (3)**, 1290–1311, doi:10.1175/MWR-D-13-00249.1, URL https://journals.ametsoc.org/mwr/article/142/3/1290/71766/Observed-Hurricane-Wind-Speed-Asymmetries-and, publisher: American Meteorological Society.

Vecchi, G. A., and Coauthors, 2019: Tropical cyclone sensitivities to CO2 doubling: roles of atmospheric resolution, synoptic variability and background climate changes. *Climate Dynamics*, **53 (9)**, 5999–6033, doi:10.1007/s00382-019-04913-y, URL https://www.dropbox.com/s/zu5uxctekjtmwj8/vecchi-tropical-2019.pdf?dl=0.

Vickery, P. J., J. Lin, P. F. Skerlj, L. A. Twisdale Jr, and K. Huang, 2006a: HAZUS-MH hurricane model methodology. I: Hurricane hazard, terrain, and wind load modeling. *Natural Hazards Review*, **7 (2)**, 82–93, publisher: American Society of Civil Engineers.

Vickery, P. J., P. F. Skerlj, J. Lin, L. A. Twisdale Jr, M. A. Young, and F. M. Lavelle, 2006b: HAZUS-MH hurricane model methodology. II: Damage and loss estimation. *Natural Hazards Review*, **7 (2)**, 94–103, publisher: American Society of Civil Engineers.

Walsh, B., and S. Hallegatte, 2020: Measuring Natural Risks in the Philippines: Socioeconomic Resilience and Wellbeing Losses. *Economics of Disasters and Climate Change*, **4 (2)**, 249–293, doi:10.1007/s41885-019-00047-x, URL https://doi.org/10.1007/s41885-019-00047-x.

Walsh, B. J., and S. Hallegatte, 2019: *Measuring Natural Risks in the Philippines: Socioeconomic Resilience and Wellbeing Losses*. The World Bank.

Watson, C. C., and M. E. Johnson, 2004: Hurricane Loss Estimation Models: Opportunities for Improving the State of the Art. *Bulletin of the American Meteorological Society*, **85 (11)**, 1713–1726, doi:10.1175/BAMS-85-11-1713, URL https://journals.ametsoc.org/view/journals/bams/85/11/bams-85-11-1713.xml, publisher: American Meteorological Society Section: Bulletin of the American Meteorological Society.

Willoughby, H. E., R. W. R. Darling, and M. E. Rahn, 2006: Parametric representation of the primary hurricane vortex. Part II: A new family of sectionally continuous profiles. *Monthly weather review*, **134 (4)**, 1102–1120.

Wilson, K., and J. W. Baldwin, 2021: Estimating Tropical Cyclone Vulnerability: A Review of Different Open-Source Approaches. *Hurricane Risk in a Changing Climate*, Springer, in Review.

World Bank, 2021: Wealth Accounting. URL https://datacatalog.worldbank.org/search/dataset/0042066.

Xi, D., N. Lin, and J. Smith, 2020: Evaluation of a Physics-Based Tropical Cyclone Rainfall Model for Risk Assessment. *Journal of Hydrometeorology*, **21 (9)**, 2197–2218, doi:10.1175/JHM-D-20-0035.1, URL https://journals.ametsoc.org/view/journals/hydr/21/9/jhmD200035.xml, publisher: American Meteorological Society Section: Journal of Hydrometeorology.

Yamin, L. E., A. I. Hurtado, A. H. Barbat, and O. D. Cardona, 2014: Seismic and wind vulnerability assessment for the GAR-13 global risk assessment. *International Journal of Disaster Risk Reduction*, **10**, 452–460, doi:10.1016/j.ijdrr.2014.05.007, URL http://www.sciencedirect.com/science/article/pii/S2212420914000466.

Yang, Q., C.-Y. Lee, M. K. Tippett, D. R. Chavas, and T. R. Knutson, 2022: Machine learning based hurricane wind reconstruction. *Weather and Forecasting*, **-1 (aop)**, doi:10.1175/WAF-D-21-0077.1, URL https://journals.ametsoc.org/view/journals/wefo/aop/WAF-D-21-0077.1/WAF-D-21-0077.1.xml, publisher: American Meteorological Society Section: Weather and Forecasting.

Yonson, R., I. Noy, and J. Gaillard, 2018: The measurement of disaster risk: An example from tropical cyclones in the Philippines. *Review of Development Economics*, **22 (2)**, 736–765, doi:10.1111/rode.12365, URL https://onlinelibrary.wiley.com/doi/abs/10.1111/rode.12365, _eprint: https://onlinelibrary.wiley.com/doi/pdf/10.1111/rode.12365.

Zscheischler, J., and Coauthors, 2018: Future climate risk from compound events. *Nature Climate Change*, 1.

LIST OF FIGURES

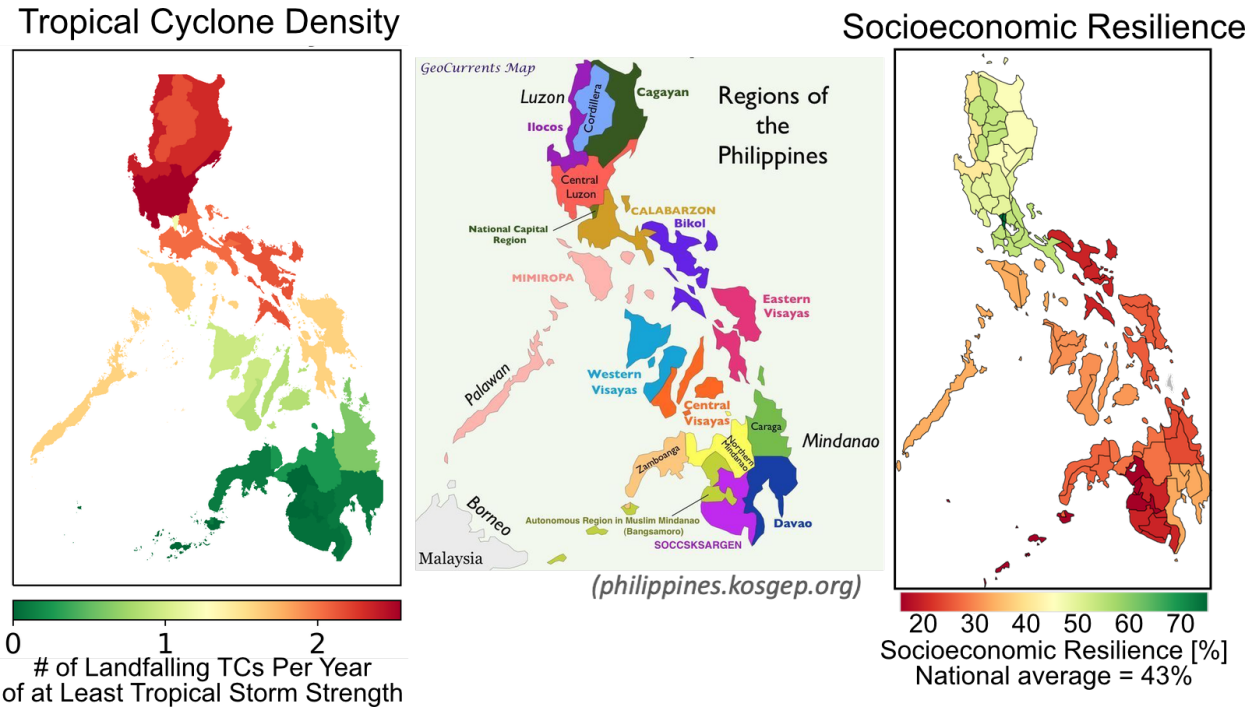

FIG. 1. **Contrasting tropical cyclone density and socioeconomic resilience in the northern versus southern Philippines.** (Left) Number of tropical storms and typhoons per year making landfall in different regions of the Philippines; (middle) map and names of regions in the Philippines (adapted from philippines.kosgep.org); (right) average socioeconomic resilience in different regions of the Philippines. Socioeconomic resilience is defined here as the ratio of expected asset losses to wellbeing losses in Walsh and Hallegatte (2020), from which the right panel of this figure is also adapted. Wellbeing losses are calculated using household survey data about consumption habits across the Philippines.

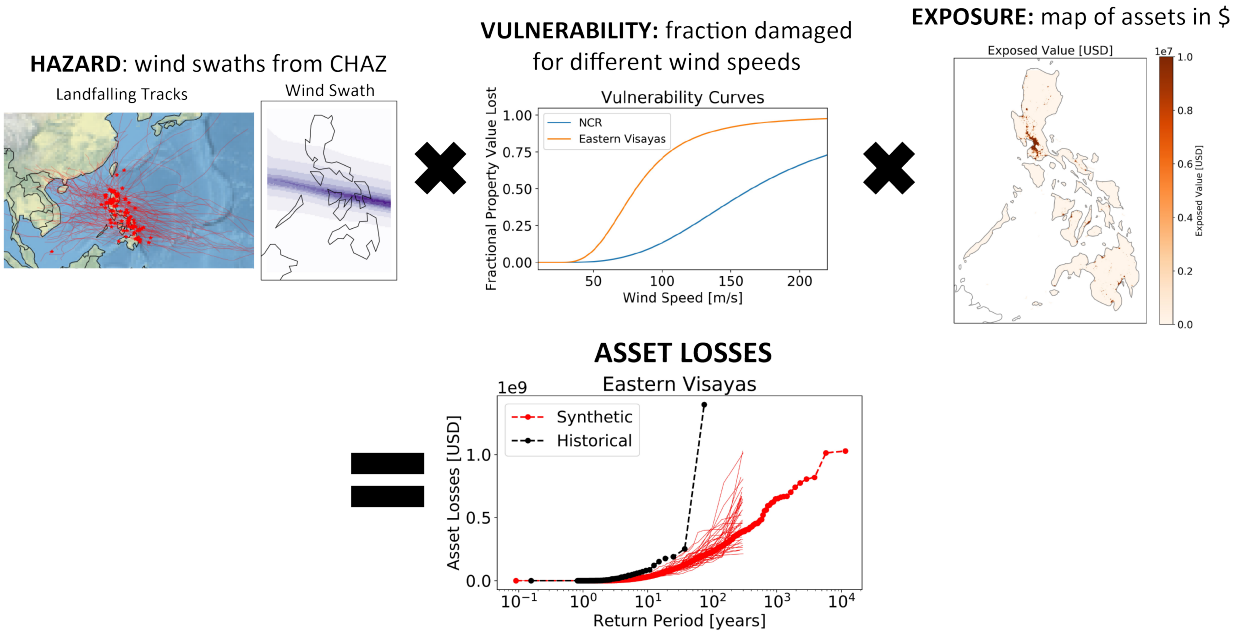

1083 FIG. 2. **Schematic of our TC risk modeling workflow.** Layers for hazard, vulnerability, and exposed value
1084 are combined to model asset losses from tropical cyclones. Details of each layer are described in Section 2.

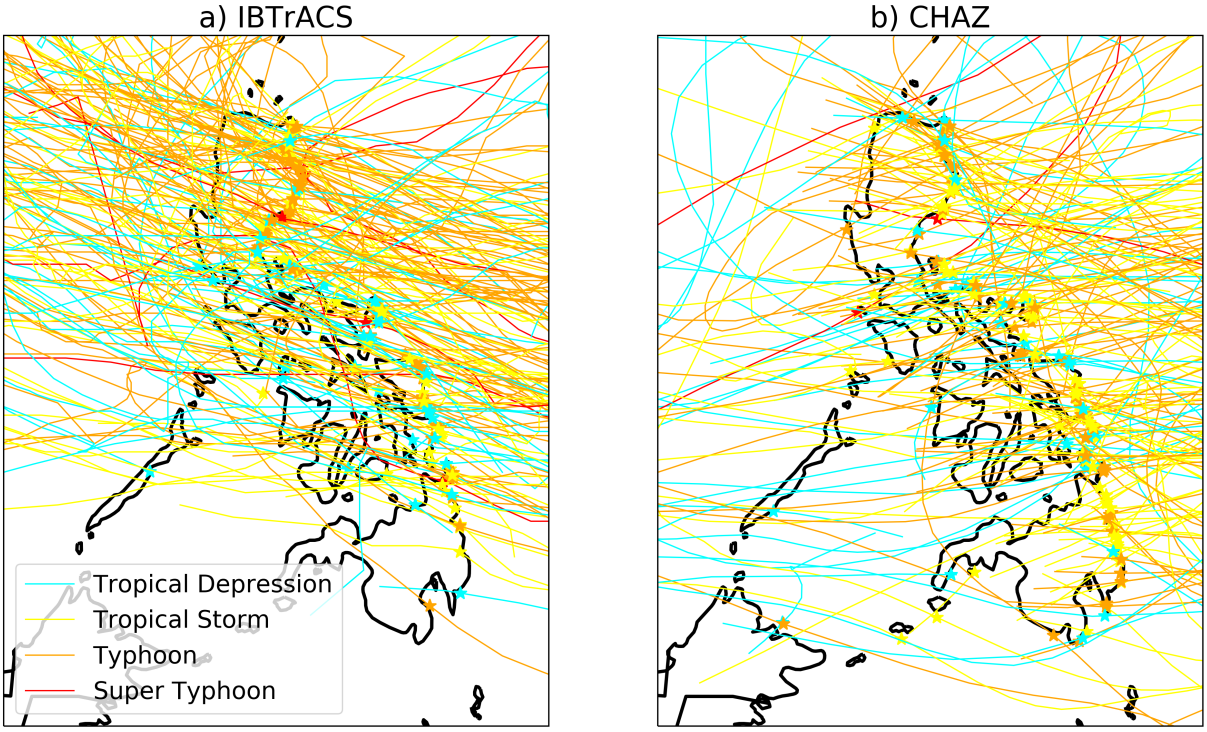

FIG. 3. **Example of observed versus synthetic landfalling TCs.** Sample of 200 landfalling TC tracks from (a) IBTrACS and (b) CHAZ. First landfall in the Philippines is demarcated with a star, and tracks are shaded by intensity at first landfall.

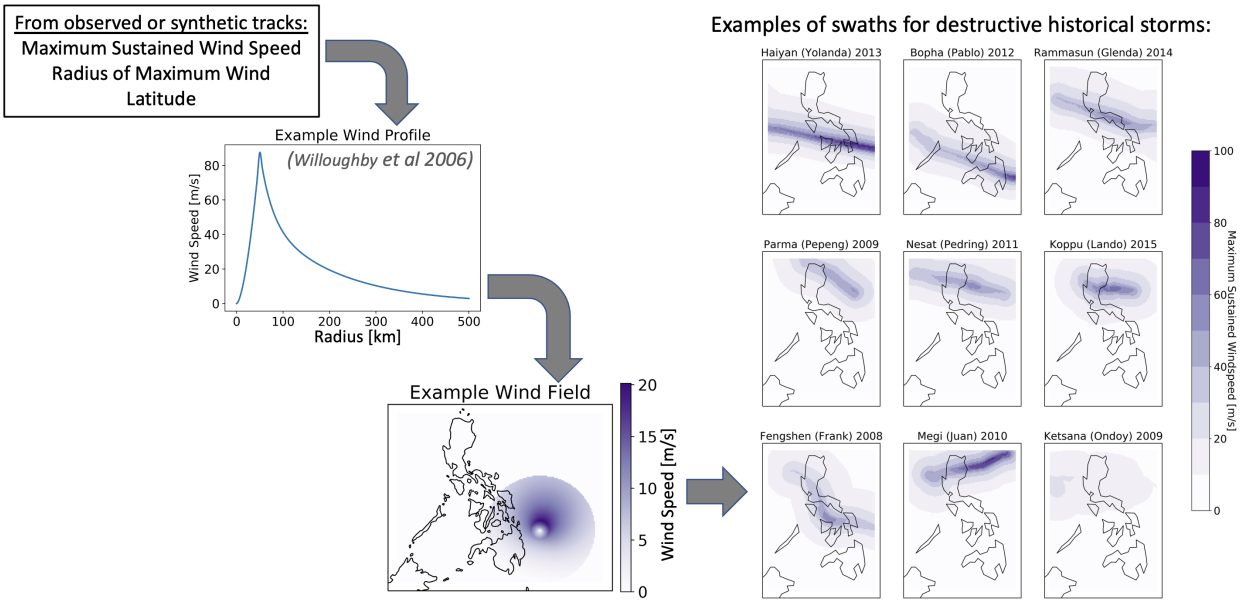

FIG. 4. **Wind swath calculation schematic and resulting swaths for highly destructive historical TCs.** Moving from left to right: 1) information on maximum sustained wind speed, latitude, and radius of maximum wind along TC tracks is used to determine 2) profiles of wind with radius from the center of the storm, which is 3) placed on a latitude-longitude grid and combined with a correction for asymmetry to determine wind fields at each point in time, then 4) the wind swath is determined as the maximum across time of the wind fields when the storm is near land. Swaths corresponding to nine of the most costly historical storms affecting the Philippines are shown on the right hand side of the figure.

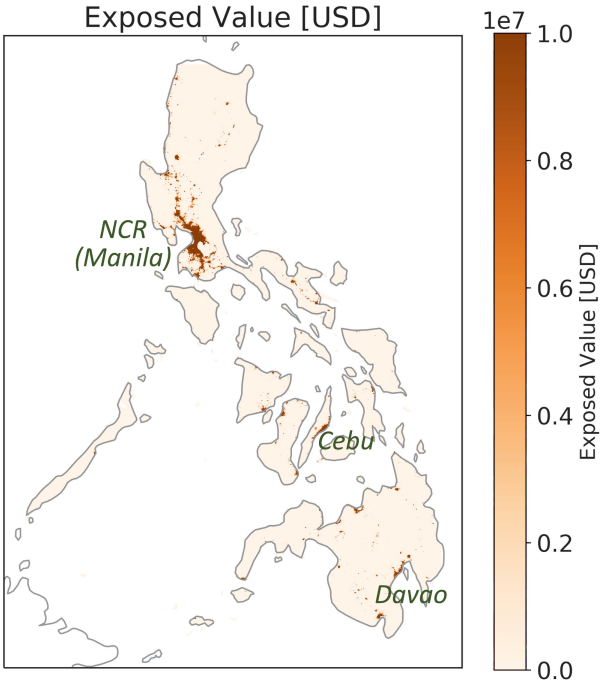

FIG. 5. **Asset value across the Philippines according to LitPop.** Shaded is the estimated value of assets in 2014 USD for each 30 arcsec gridcell of LitPop. Major cities with high concentraion of assets are labeled.

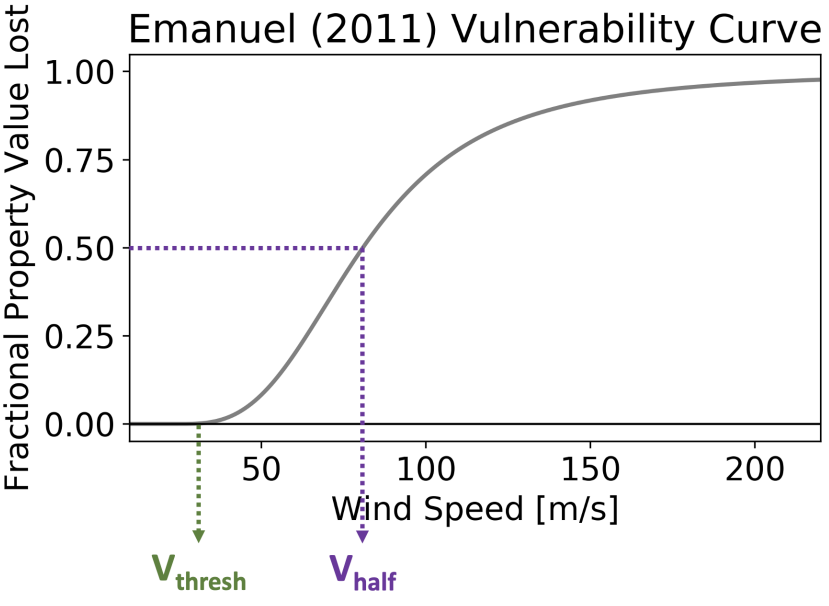

FIG. 6. **Example vulnerability curve based on Emanuel (2011).** Indicated are the two parameters that constrain the vulnerability curve: V_{thresh} (the minimum wind speed to have any damages) and V_{half} (the wind speed at which 50% of property value is lost).

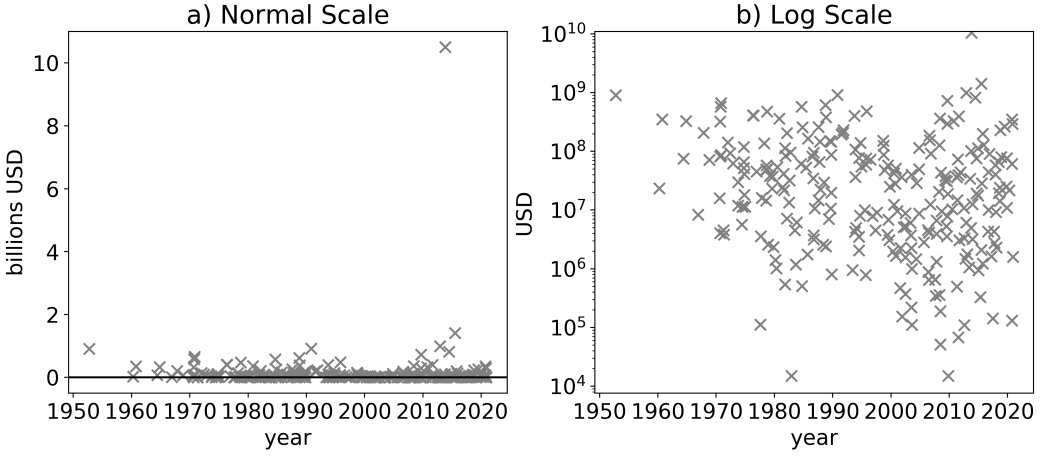

FIG. 7. **Historical TC-related damages for the Philippines over time from EM-DAT.** (a) has a linear y-axis and (b) has a log-scale y-axis, highlighting the many orders of magnitude damages from these events span.

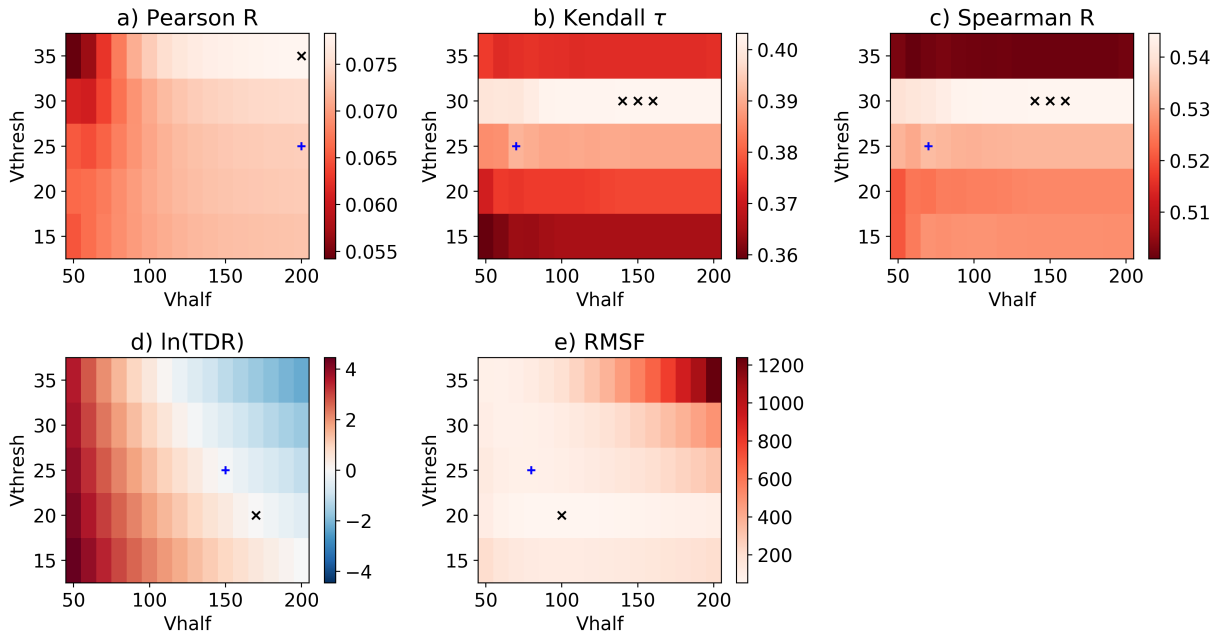

FIG. 8. **Sensitivity test of model ability to simulate historical damages considering different vulnerability parameter values (V_{half} and V_{thresh}) in the Emanuel (2011) vulnerability curve.** The metrics evaluated are (a) Pearson's r, (b) Kendall's τ, (c) Spearman's r, (d) TDR (the natural logarithm of this quantity is shown), and (e) RMSF. For all panels, whiter shading indicates better correlation. Black X's demarcate the optimal parameter values for each metric across all V_{half} and V_{thresh} values, and blue crosses demarcate the optimal V_{half} parameter value when V_{thresh} is set to 25 m/s. Panels with multiple black X's indicate optimal parameter sets with equivalent correlation.

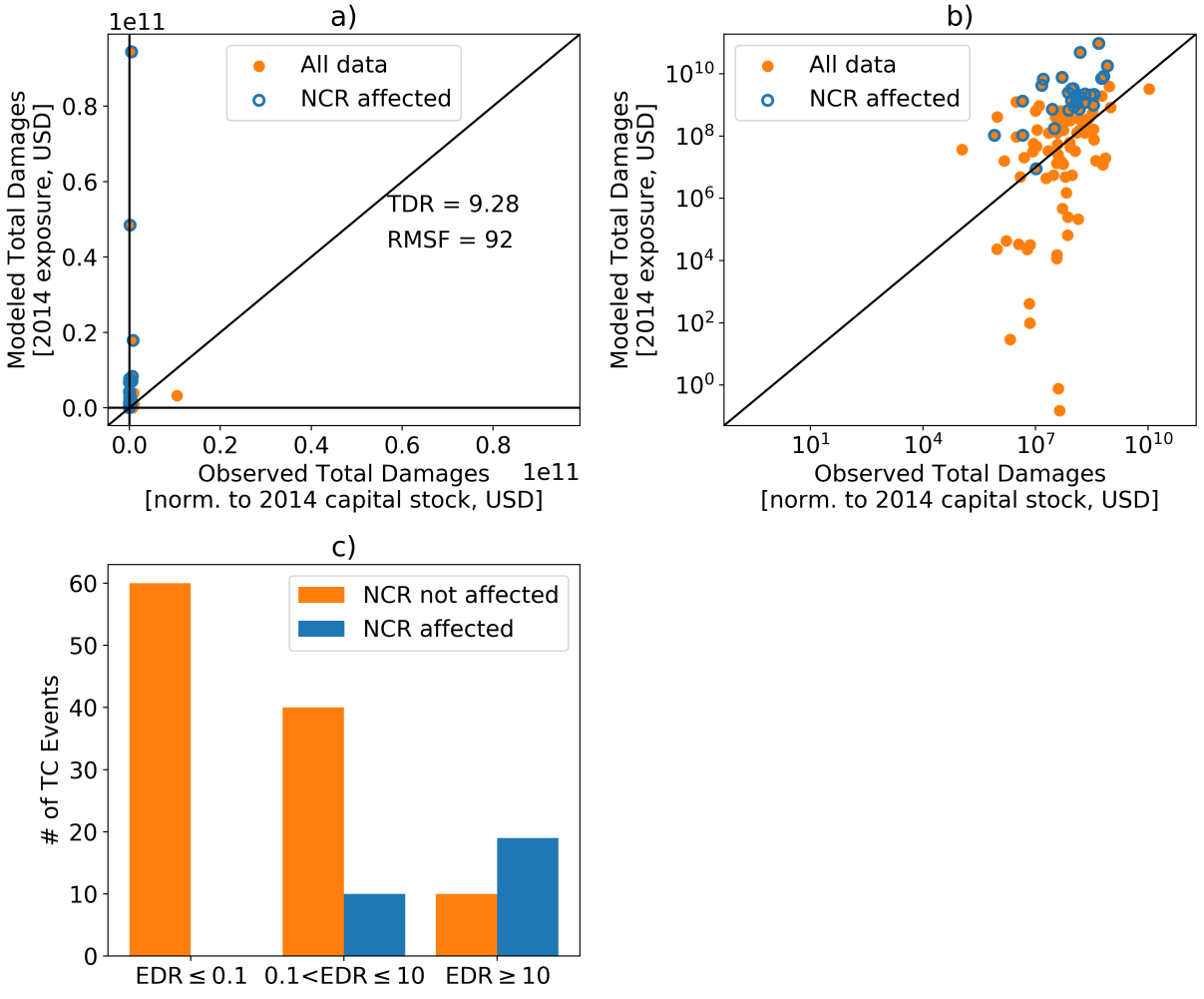

FIG. 9. **Simulated versus observed asset losses with a single national vulnerability curve fit to minimize RMSF.** Observed total damages are plotted against modeled total damages with (a) linear axes and (b) log-scale axes (b); black lines are one-to-one lines and events that result in losses in Manila are encircled in blue. (c) Bar chart of number of TC events with damage ratios less than 0.1, between 0.1 and 10, and greater than 10, split into events that do not affect Manila (orange) versus those that do affect Manila (blue). As a reminder, event damage ratio is equal to simulated damages for a TC divided by normalized reported damages for the same TC.

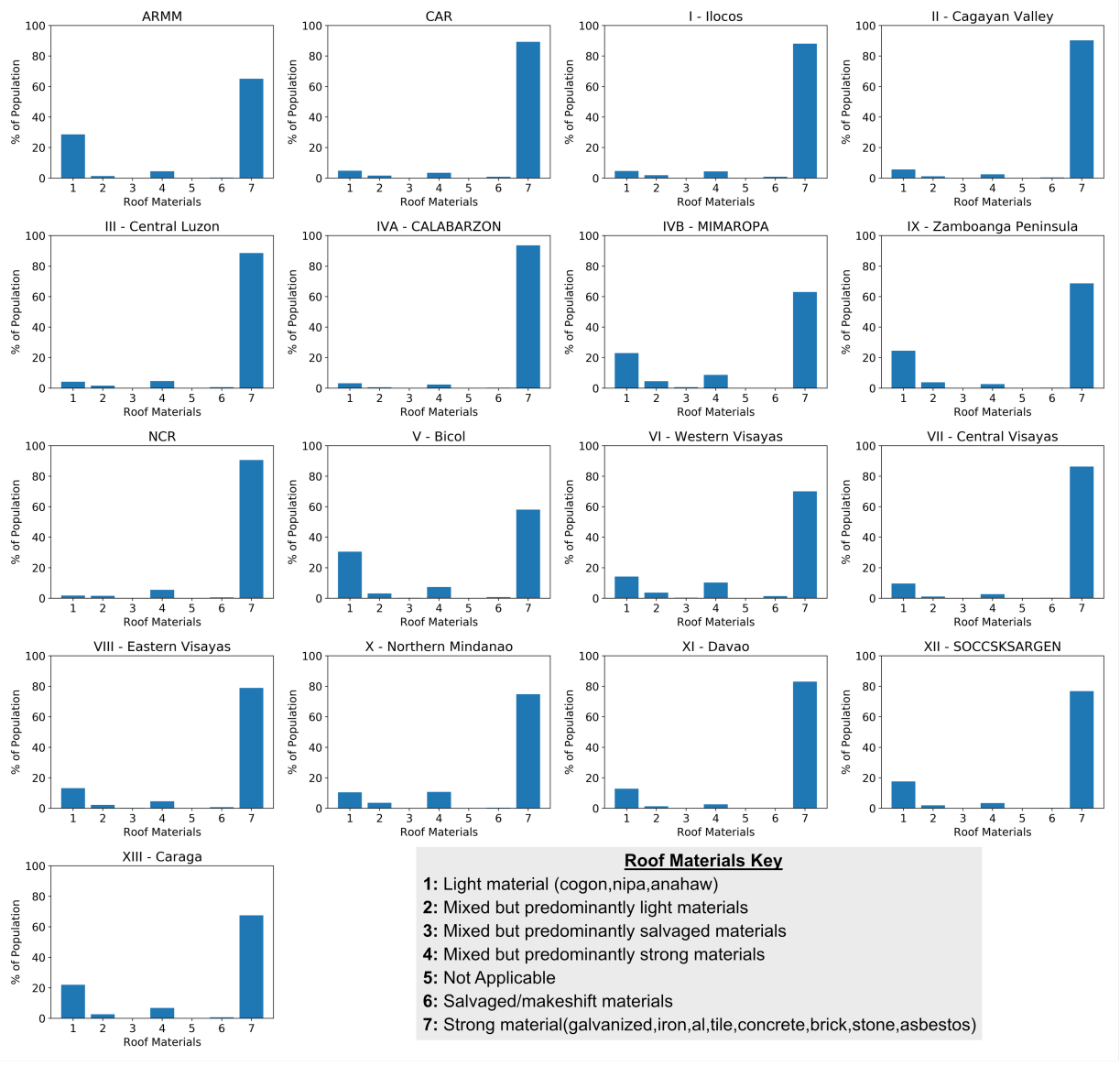

FIG. 10. **Prevalence of different roof materials for regions in the Philippines.** Bar charts for each region showing percent of population occupying dwellings made of different roof materials, according to the Philippines household survey data (FIES). The key in grey shows what roof materials each x-axis number represents.

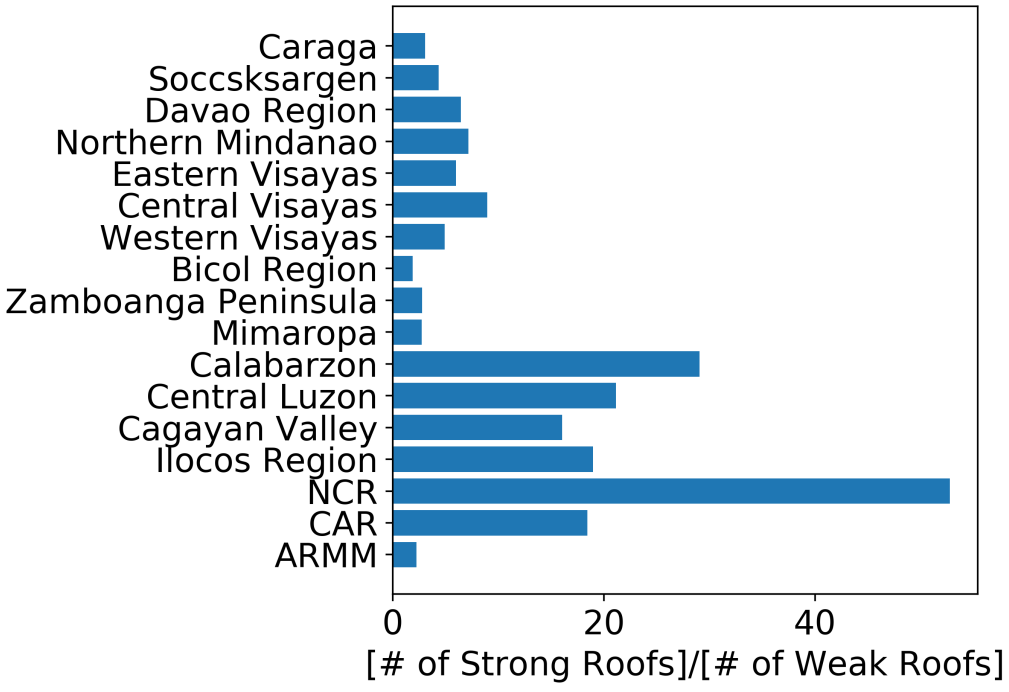

FIG. 11. **Proportion of strong to weak roofs for regions in the Philippines.** Bar chart showing number of strong divided by number of light roofs for each region in the Philippines.

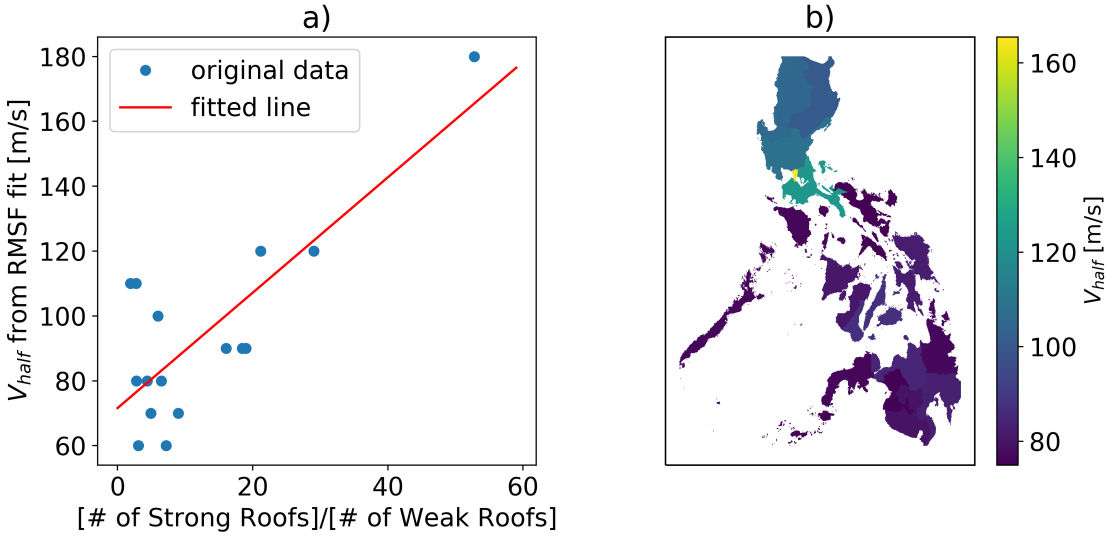

FIG. 12. **Correspondence of regional V_{half} to roof strength proportion, and resulting vulnerability map from regression.** (a) Proportion of strong to weak roofs plotted against RMSF fitted regional V_{half} values (blue circles) and linear fit between the two quantities (red line); (b) regional V_{half} determined from proportion of strong to weak roofs in each province and linear fit in panel a. Note that in panel a, NCR is the top-right point in the plot with the highest V_{half} and strong roof proportion.

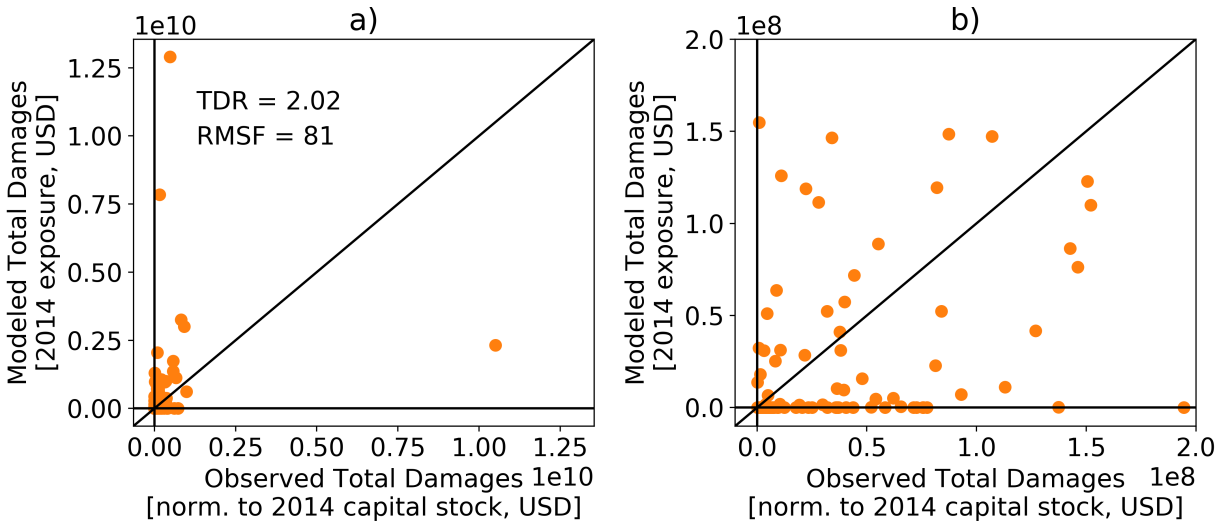

FIG. 13. **Observed versus modeled damages for regionally varying vulnerability.** (a) Observed total damages from EM-DAT plotted against modeled total damages calculated with the regional varying vulnerability map; black line is the one-to-one line. (b) Same as panel a but with reduced x and y-axis limits to highlight the prevalence of storms with zero modeled damages.

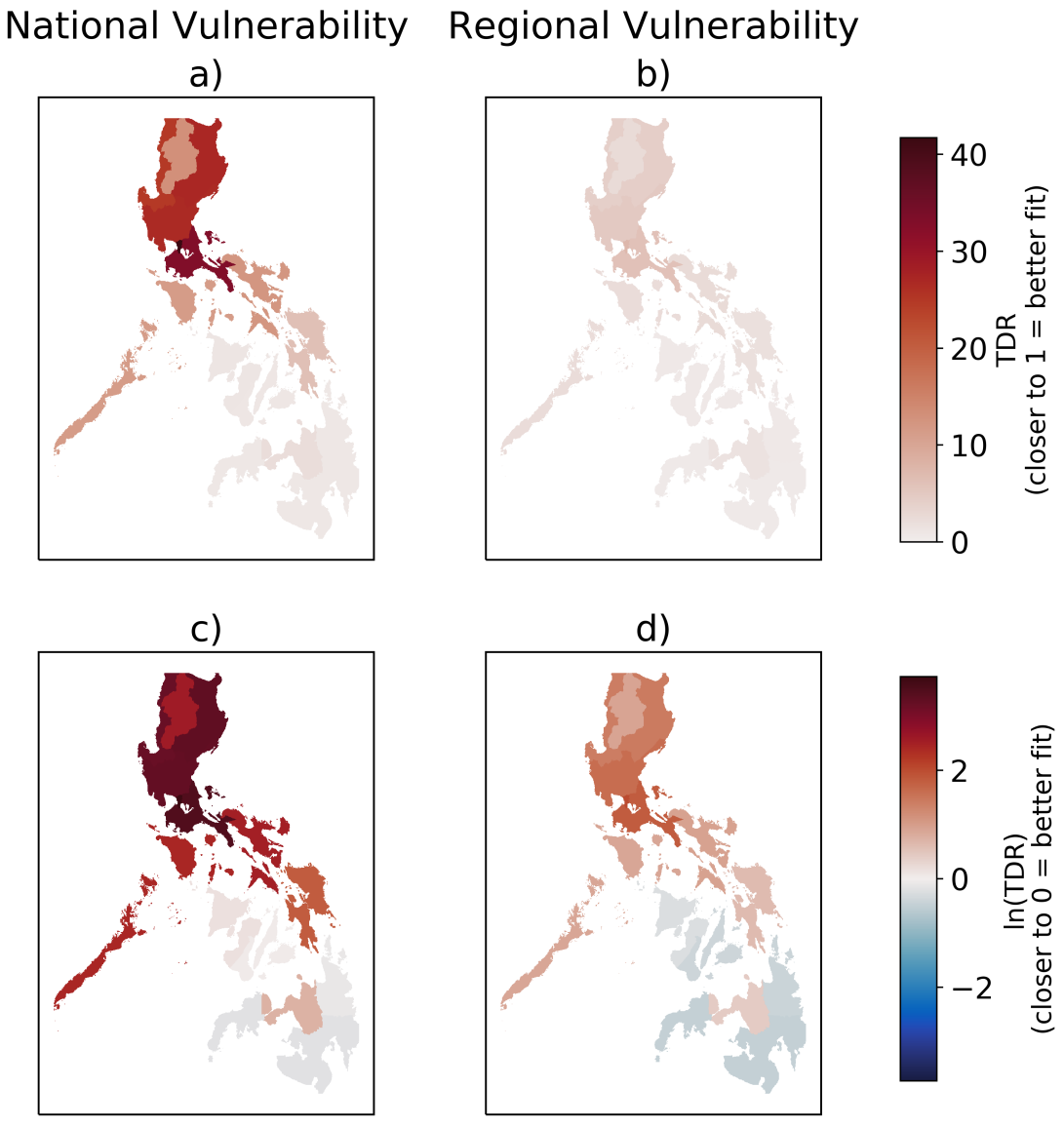

1129 FIG. 14. **Damage simulation skill for national versus regionally varying vulnerability.** TDR across regions
1130 for single national vulnerability curve (left) and regionally varying vulnerability curves (right) and quantified as
1131 raw TDR (top) versus natural log of TDR (bottom).

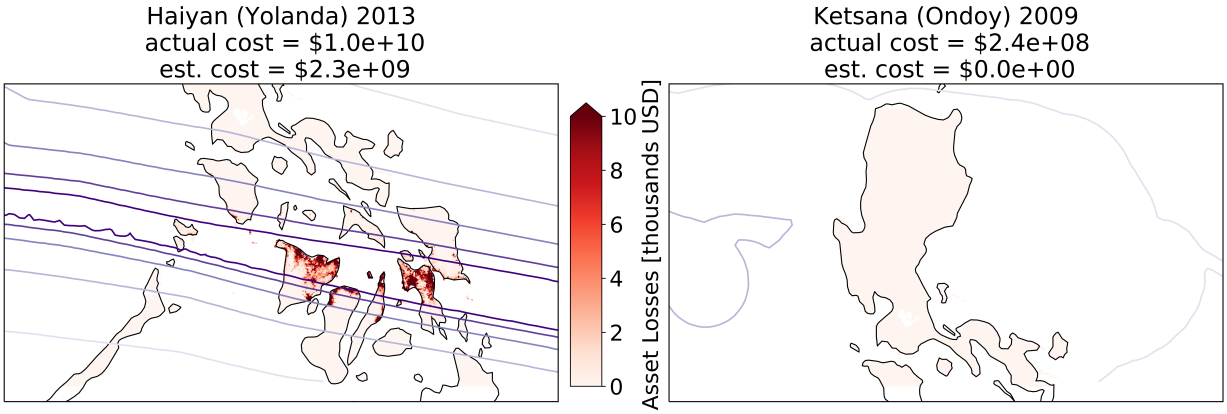

FIG. 15. **Wind swath and asset losses for two notable Philippines-landfalling typhoons.** Wind swath (contoured in purple— darker contours corresponds to faster wind speeds) and damages (shaded red) for (left) typhoon Haiyan (Yolanda) and (right) Ketsana (Ondoy). The plot region is constrained to the area of most direct impact by each storm, and at the top of each plot the actual cost from EM-DAT is listed above the simulated damages summed across the entire Philippines.

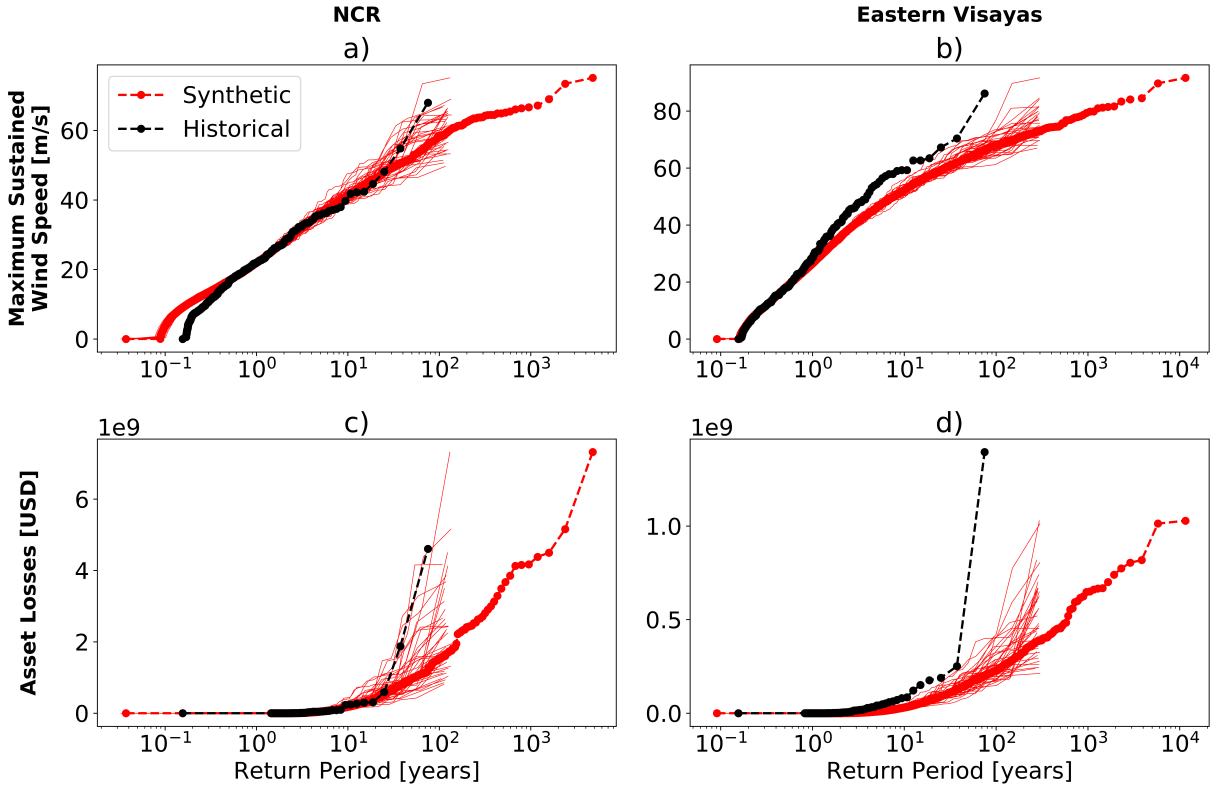

FIG. 16. **Return periods for wind speed and asset losses for two regions in the Philippines.** Return periods of different (top) maximum sustained wind speeds and (bottom) asset losses, for two regions: (left) Manila/NCR and (right) Eastern Visayas. Simulated damages from IBTrACS tracks are shown in black, while simulated damages from CHAZ tracks are shown in red; the thin red lines designate return periods derived from each CHAZ intensity ensemble while the thick dashed red line shows return periods from all the CHAZ tracks and intensity ensembles together.